Accepted Manuscript

Development of alkyl glycerone phosphate synthase inhibitors: Structure-activity relationship and effects on ether lipids and epithelial-mesenchymal transition in cancer cells

Giulia Stazi, Cecilia Battistelli, Valentina Piano, Roberta Mazzone, Biagina Marrocco, Sara Marchese, Sharon M. Louie, Clemens Zwergel, Lorenzo Antonini, Alexandros Patsilinakos, Rino Ragno, Monica Viviano, Gianluca Sbardella, Alessia Ciogli, Giancarlo Fabrizi, Roberto Cirilli, Raffaele Strippoli, Alessandra Marchetti, Marco Tripodi, Daniel K. Nomura, Andrea Mattevi, Antonello Mai, Sergio Valente

PII: S0223-5234(18)31009-2

DOI: https://doi.org/10.1016/j.ejmech.2018.11.050

Reference: EJMECH 10908

To appear in: *European Journal of Medicinal Chemistry*

Received Date: 24 July 2018

Revised Date: 6 November 2018

Accepted Date: 20 November 2018

Please cite this article as: G. Stazi, C. Battistelli, V. Piano, R. Mazzone, B. Marrocco, S. Marchese, S.M. Louie, C. Zwergel, L. Antonini, A. Patsilinakos, R. Ragno, M. Viviano, G. Sbardella, A. Ciogli, G. Fabrizi, R. Cirilli, R. Strippoli, A. Marchetti, M. Tripodi, D.K. Nomura, A. Mattevi, A. Mai, S. Valente, Development of alkyl glycerone phosphate synthase inhibitors: Structure-activity relationship and effects on ether lipids and epithelial-mesenchymal transition in cancer cells, *European Journal of Medicinal Chemistry* (2018), doi: https://doi.org/10.1016/j.ejmech.2018.11.050.

Cancer specificity: no toxic effect in non-malignant human mesothelial MeT5A cells

↓ 50-70% ether lipids
↓ 78% cell migration in aggressive 231MFP breast cancer cells

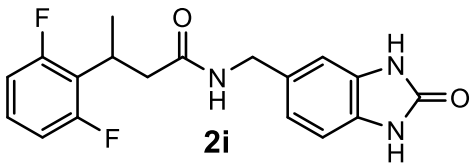

2i

EMT modulation:
↑ E-cadherin
↓ Snail and MMP2
mRNA levels in PC-3 prostate and MDA-MB-231 breast cancer cells

AGPS binding (X ray crystallography) and inhibition (ThermoFAD and radioactivity assays)

Development of Alkyl Glycerone Phosphate Synthase Inhibitors: Structure-Activity Relationship and Effects on Ether Lipids and Epithelial-Mesenchymal Transition in Cancer Cells

Giulia Stazi[a,1], Cecilia Battistelli[b,1], Valentina Piano[c,d,1], Roberta Mazzone[a,e], Biagina Marrocco[c], Sara Marchese[c], Sharon M. Louie[f], Clemens Zwergel[a], Lorenzo Antonini[g], Alexandros Patsilinakos[a], Rino Ragno[a], Monica Viviano[h], Gianluca Sbardella[h], Alessia Ciogli[a], Giancarlo Fabrizi[a], Roberto Cirilli[i], Raffaele Strippoli[b,j], Alessandra Marchetti[b], Marco Tripodi[b,j,k], Daniel K. Nomura[f], Andrea Mattevi[c,]*, Antonello Mai[a,k,]*, and Sergio Valente[a,]*

[a]Department of Chemistry and Technologies of Drugs, Sapienza University of Rome, P. le A. Moro 5, 00185 Rome, Italy

[b]Department of Molecular Medicine, Sapienza University of Rome, Viale Regina Elena 324, 00161 Rome, Italy

[c]Department of Biology and Biotechnology, University of Pavia, Via Ferrata 9, 27100 Pavia, Italy

[d]Department of Mechanistic Cell Biology, Max-Planck Institute of Molecular Physiology, Otto-Hahn-Str. 11, 44227 Dortmund, Germany

[e]Center for Life Nano Science@Sapienza, Italian Institute of Technology, Via Regina Elena 291, 00161 Rome, Italy

[f]Departments of Chemistry, Molecular and Cell Biology, and Nutritional Sciences and Toxicology, University of California, Berkeley, Berkeley, CA 94720 USA

[g]Alchemical Dynamics s.r.l. 00125 Rome, Italy

[h]Department of Pharmacy, Epigenetic Med Chem Lab, University of Salerno, via Ponte Don Melillo, 84084 Fisciano (SA), Italy

[i]Centro Nazionale per il Controllo e la Valutazione dei Farmaci, Istituto Superiore di Sanità, Viale Regina Elena 299, I-00161 Rome , Italy

[j]Gene Expression Laboratory, National Institute for Infectious Diseases "Lazzaro Spallanzani" I.R.C.C.S., Rome, Italy

[k]Pasteur Institute - Cenci Bolognetti Foundation, Sapienza Università di Roma, Viale Regina Elena 324, 00161 Rome, Italy

KEYWORDS (AGPS inhibitors, ether lipids, cancer, E-cadherin, Snail)

ABSTRACT: In aggressive tumors, alkylglyceronephosphate synthase (AGPS) controls cellular ether phospholipid utilization and metabolism to promote cancer cell proliferation and motility. SAR studies on the first-in-class AGPS inhibitor **1,** discovered by our group, led to the 2,6-difluoro analog **2i** which showed higher binding affinity than **1** *in vitro*. In 231MFP cancer cells, **2i** reduced ether lipids levels and cell migration rate. When tested in PC-3 and MDA-MB-231 cancer cells, **2i** specifically impaired epithelial to mesenchymal transition (EMT) by modulating E-cadherin, Snail and MMP2 expression levels. Moreover, the combination of siRNAs against AGPS and **2i** provided no additive effect, confirming that the modulation of **2i** on EMT specifically relies on AGPS inhibition. Finally, this compound also affected cancer cell proliferation especially in MDA-MB-231 cells expressing higher AGPS level, whereas it provided negligible effects on MeT5A, a non-tumorigenic cell line, thus showing cancer specificity.

INTRODUCTION

Aggressive metastatic tumors exhibit an altered cell metabolism favoring increased cell proliferation rate and invasiveness. Among the metabolic processes involved in cancer development, aberrant lipid metabolism and enhanced *de novo* lipogenesis play an essential role in promoting cell division and motility.[1-3] Although the physiological role of ether lipids is not fully understood, many findings suggest their implication in driving cancer pathogenicity by contributing to free radical scavenging, cell motility, cell membrane plasticity and vesicle formation, and generation of oncogenic lipid signaling molecules.[4, 5] The critical step in ether phospholipid synthesis is catalyzed by the peroxisomal flavoenzyme alkylglyceronephosphate synthase (AGPS).[6] AGPS enables the acyl/alkyl exchange of the substrate acyl-dihydroxyacetone phosphate (acyl-DHAP), using the flavin cofactor (FAD) through an unusual non-redox catalytic mechanism. Indeed, the FAD covalently binds the DHAP moiety of acyl-DHAP, acting as a trap to immobilize the substrate and allows the exchange of the fatty acid chain of acyl-DHAP with a fatty alcohol substrate, forming the precursor of all ether lipid species.[3, 6-8] It has been shown that AGPS is up-regulated across different types of aggressive and metastatic tumors, such as human breast, melanoma and prostate cancers.[3, 7-10] To elucidate the contribution of AGPS to cancer pathogenicity, the gene encoding for the enzyme was genetically silenced in breast 231MFP and melanoma C8161 cancer cell lines. Its inactivation led to an overall reduced level of multiple structural ether lipids, as well as oncogenic signaling molecules, such as

lysophosphatidic acid ethers (LPAe), platelet activating factor ethers (PAFe) and eicosanoids, which contribute to the inflammatory microenvironment.[11]

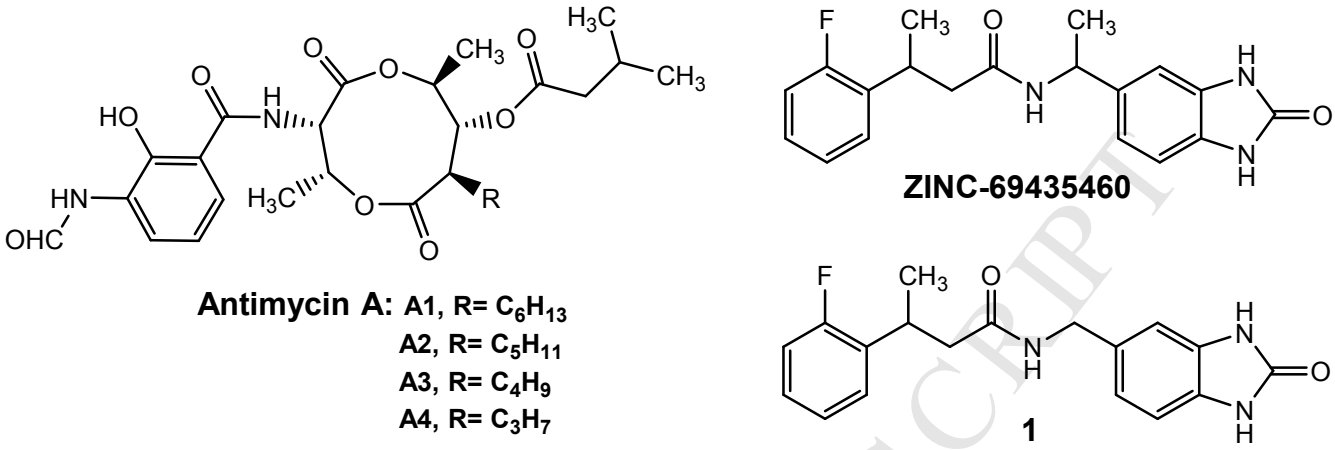

Chart 1. First disclosed inhibitors of AGPS

As AGPS knockdown showed remarkable effects on tumor growth in a xenograft mouse model,[3] we implemented a small molecule screening to identify the first compounds able to reproduce the phenotype induced by AGPS silencing. We identified Zinc-69435460 (3-(2-fluorophenyl)-*N*-(1-(2-oxo-2,3-dihydro-1*H*-benzo[*d*]imidazol-5-yl)ethyl)butanamide) and antimycin A (Chart 1) as first AGPS inhibitors.[12, 13] High resolution X-ray structure of the AGPS/Zinc-69435460 complex highlighted a detailed view of the inhibitor binding mode, with all the three inhibitor moieties (fluorophenyl, propanamide, and dihydrobenzoimidazole) involved in specific interactions with the surrounding protein/amino acid residues and with the FAD cofactor. Compound **1**, the analog of Zinc-69435460 lacking one of the two racemic methyl groups (Chart 1), showed higher binding affinity and the same inhibitory effect as the prototype, thus it was chosen as lead compound for further biological evaluation. In C8161 melanoma, 231MFP breast, and SKOV3 ovarian cancer cell lines **1** was able to selectively lower ether lipid levels as well as to induce a 50% reduction of cell survival and migration rate.[13]

Here, we present some SAR investigation on the **1** scaffold aimed to pinpoint the main structural requirements for AGPS inhibition, and to improve the potency in both enzyme and cellular assays. A

variant of the ThermoFluor assay, ThermoFAD, measuring the unfolding temperature of the protein by monitoring the increase in FAD fluorescence upon release from the protein, performed on the **1** analogs highlighted the 2,6-difluoro compound **2i** as the most effective AGPS binder. This ability has been confirmed by the X-ray structure of the complex AGPS/**2i**. The **2i** inhibitory effect was validated by an *in vitro* radioactivity-based enzymatic assay and in 231MFP cancer cells where it was lowering ether lipids and cell migration rate. Finally, the effects of genetic (siRNAs) and/or pharmacological (**1** and **2i**) AGPS inhibition on epithelial-mesenchymal transition (EMT) in prostate PC-3 and breast MDA-MB-231 cancer cells have been assessed.

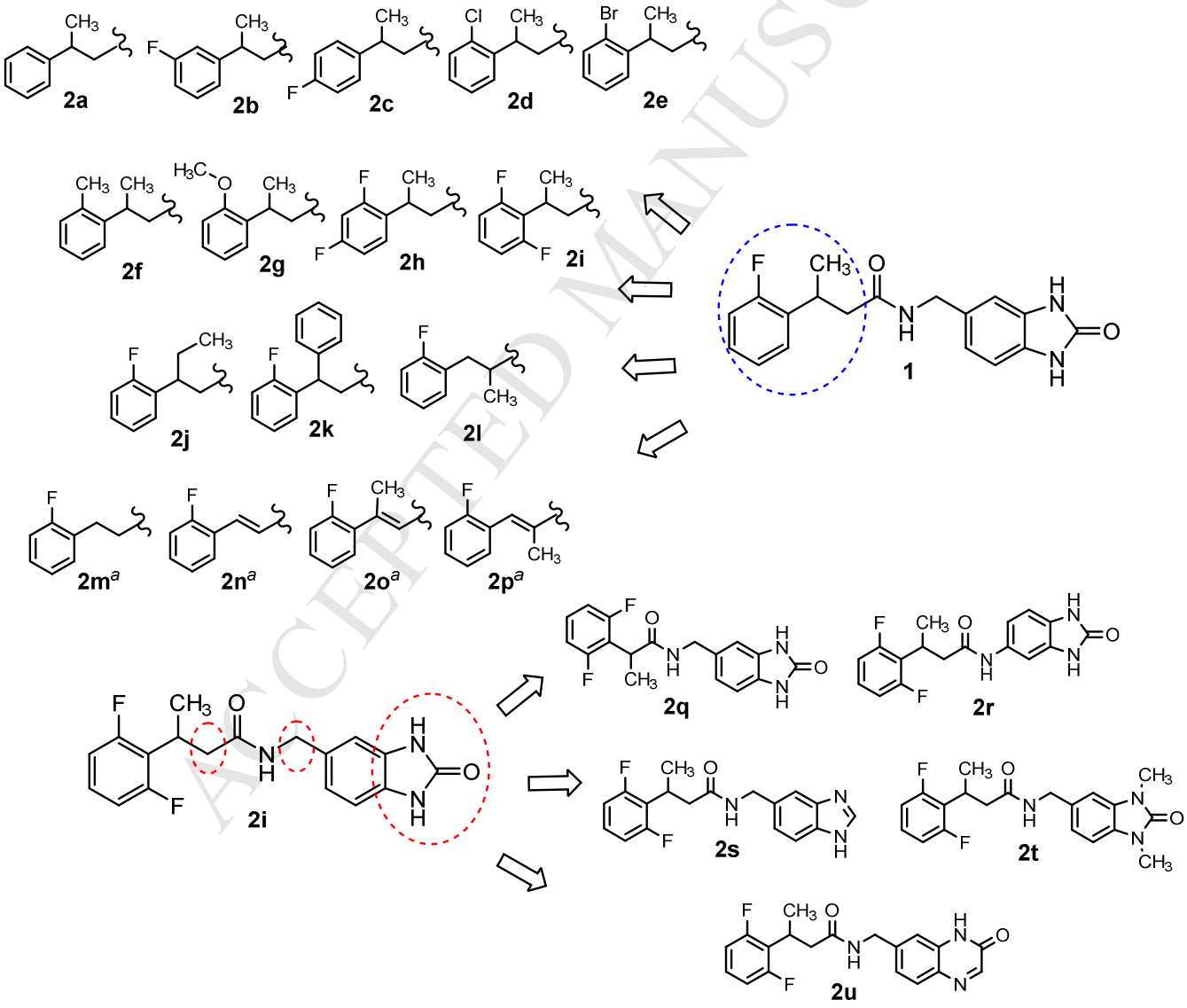

Figure 1. Development of novel AGPS inhibitors **2a-l, q-u**. [a]Ref. 13.

RESULTS AND DISCUSSION

Chemistry

We performed chemical manipulations on the **1** structure (Figure 1) including: i) removal or shift of the 2-fluoro substituent to the 3- or 4-position of the phenyl ring (**2a**-**c**); ii) replacement of the 2-fluoro with other substituents such as different halogens (**2d**,**e**), methyl or methoxy (**2f**,**g**), or double-fluoro substitution (**2h**,**i**); iii) introduction of groups bulkier than methyl at the propionamide β-carbon (**2j**,**k**); iv) shift of the methyl group from the propionamide β- to α-position (**2l**). The effect of removal of the propionamide β-methyl group and/or unsaturation of the propionamide chain and eventual insertion of a methyl group at the α-unsaturated position (**2m**-**p**) has been already reported as at least in part detrimental for the AGPS binding activity.[13]

From this first round of synthesis and screening (ThermoFAD analysis), the 2,6-difluoro analog **2i** clearly emerged as the most potent compound. Therefore, we further modified its structure by v) shortening the propanamide or the aminomethyl dihydrobenzoimidazole chain (**2q**,**r**); vi) replacing the 2-oxo-2,3-dihydro-1*H*-benzo[*d*]imidazole with 1*H*-benzo[*d*]imidazole (**2s**), 1,3-dimethyl-2-oxo-2,3-dihydro-1*H*-benzo[*d*]imidazole (**2t**), or 3-oxo-3,4-dihydroquinoxaline (**2u**) (Figure 1).

The synthesis of derivatives **2a-l**,**r-u** started from Wittig-Horner condensation between differently substituted ketones and trimethyl phosphonoacetate by using 60% sodium hydride in tetrahydrofuran at 0 °C, or alternatively between 2-fluorobenzaldehyde and triethyl 2-phosphonopropionate with anhydrous potassium carbonate in ethanol at 80 °C, to afford the unsaturated esters **3a-d, 3f-l**. Such esters (**3a-d, 3f-l**) were then saturated through palladium catalyzed hydrogenation in methanol by using a ThalesNano H-Cube Reactor to afford the corresponding propionic methyl esters **4a-l**, wherein compound **4e** was commercially available. The esters **4a-l** were converted to the corresponding carboxylic acids **5a-l** through basic hydrolysis (2N potassium hydroxide in ethanol). The 2-(2,6-difluorophenyl)propanoic acid **5m** was prepared according to the literature.[14] The acids **5a-m**

were finally coupled with the opportune amines **6-10** [see Supporting Information (SI) for their preparation] by using *N*,*N*-carbonyldiimidazole and triethylamine in anhydrous *N*,*N*-dimethylformamide to obtain the final amides **2a-l,q-u** (Scheme 1).

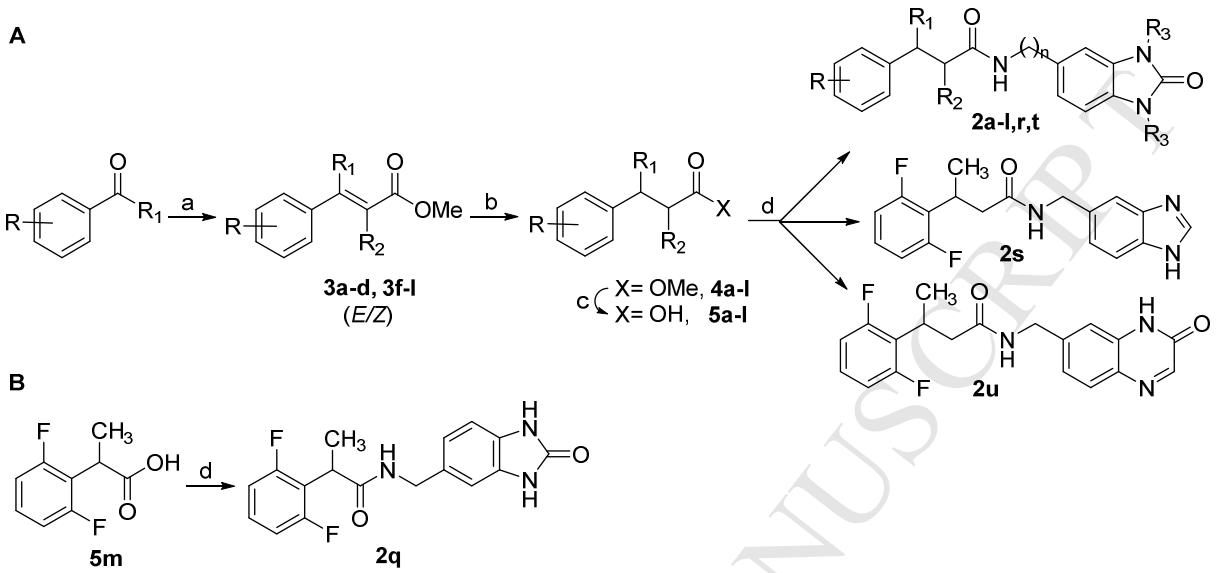

Scheme 1. Synthesis of compounds **2a-l, q-u.** *Reagents and conditions:* a) trimethyl phosphonoacetate, 60% NaH, dry THF, 0 °C to rt, N_2 atmosphere, overnight (41-79%); or triethyl 2-phosphonopropionate, dry K_2CO_3, dry EtOH, 80 °C, 2 h; b) MeOH, 10% Pd/C, P_{H2}=10 bar, v=1 mL/min, 30 °C (79-83%); c) 2N KOH, EtOH, rt, overnight (94-97%); d) appropriate amine among **6-10**, *N*,*N*-carbonyldiimidazole, dry DMF, rt or 70 °C, overnight (73-85%). The exact structures of compounds **3-5** are reported in SI.

ThermoFAD screening of compounds 2a-l, q-u

We recently showed that ThermoFAD was a reliable assay to screen AGPS-binding molecules.[13] Data determined with **2a-u** (Table 1) clearly showed the crucial role of the fluoro (compare the thermal shift (Tm) of **1**, **2b**-**c** with that of **2a**) or other halogens or methyl group (see **2d**-**f**) to have great binding affinity. Indeed, the deletion of the fluorine at C2 position (**2a**) resulted in a decrease of Tm (+ 1.5 °C) when compared with the reference **1** (+ 3.5 °C), whereas its replacement with other halogens, such as chlorine (**2d**), bromine (**2e**) or with a methyl group (**2f**) was well tolerated, showing Tm values for these compounds similar to the reference **1**.

Contrarily, the introduction of the methoxy group (**2g**) abrogated the AGPS binding of the compound. When the fluoro atom was shifted to *meta* or *para* position on the phenyl ring (**2b** and **2c**, respectively) the *meta*-substitution (**2b**) gave a weak decrease of Tm value (+ 3.0 °C), whereas the *para*-substitution (**2c**) provided a slight (weak) increase in Tm value (+ 4.0 °C). Hence, we also performed the double insertion of 2,4- and 2,6-difluoro substitution (**2h** and **2i**) at the phenyl ring, that resulted in a stronger enzyme binding, with the 2,6-difluoro derivative **2i** giving the highest increase of Tm (+ 5 °C). An increase of the steric hindrance at the propionamide β–position with an ethyl (**2j**) or phenyl (**2k**) substituent caused a decrease or complete loss in AGPS binding, respectively, whereas the shift of the methyl group from the propionamide β- to the α-carbon atom (**2l**) was fully tolerated. As already reported,[13] the removal of the β-methyl group (**2m**) or the unsaturation of the propionamide chain (**2n**,**o**) led to a loss of binding activity, in part restored by insertion of an α-methyl group (**2p**). Based on these results, we further explored the **2i** structure to acquire more SAR data. The additional attempts to shorten the distance between the phenyl (**2q**) or the dihydrobenzoimidazole (**2r**) portion and the amide moiety provided compounds with very weak or no AGPS binding, respectively, thus showing that the length of the molecule and, in particular, the distance between the two aromatic moieties is a crucial point. Furthermore, the double methylation of the dihydrobenzoimidazole ureidic nitrogens (**2s**), or its replacement with a benzoimidazole heterocycle (**2t**) or with a 3-oxo-3,4-dihydroquinoxaline ring (**2u**) were not tolerated, showing no protein-inhibitor interaction.

Table 1
TermoFAD data of compounds **2a-u**[a]

Cpd	Molecular structure	Tm, °C)	Cpd	Molecular structure	Tm, °C)
1	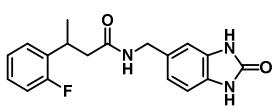	+3.5	**2k**	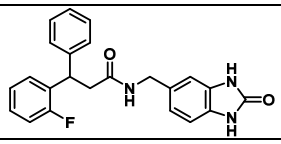	0

2a	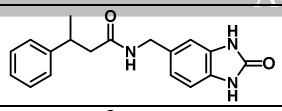	+1.5	**2l**	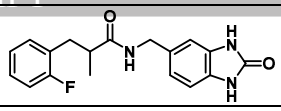	+3.0
2b	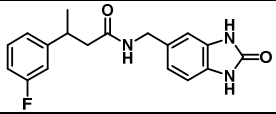	+3.0	**2m**[b]	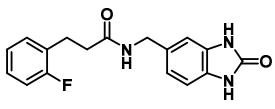	0
2c	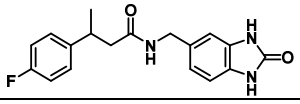	+4.0	**2n**[b]	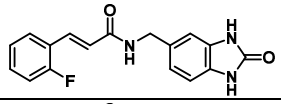	0
2d	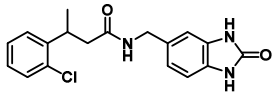	+3.5	**2o**[b]	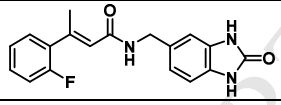	0
2e	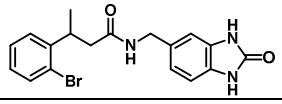	+3.5	**2p**[b]	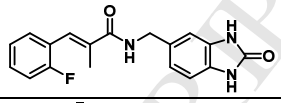	+2.0
2f	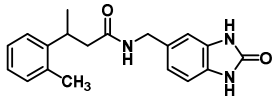	+3.0	**2q**	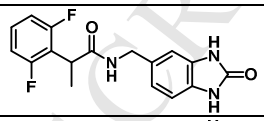	+1
2g	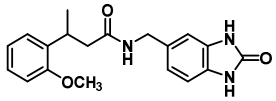	0	**2r**	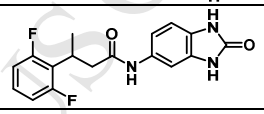	0
2h	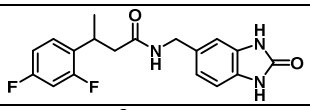	+3.5	**2s**	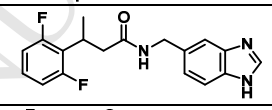	0
2i	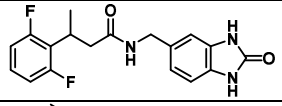	+5	**2t**	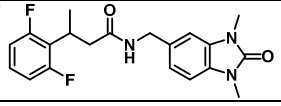	0
2j	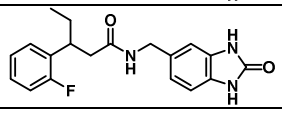	+1	**2u**	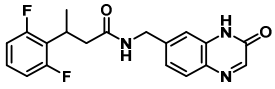	0

[a]All experiments were performed in triplicate; SD, standard deviations are within ±0.5°C; [b]Ref. 13

Crystallographic studies of AGPS/2i complex

The three-dimensional structure of AGPS in complex with **2i** was determined by X-ray crystallography (2.7 Å) (Table 2). The binding mode of **2i** is identical to that previously reported for **1** (the (*S*) configuration has been tentatively assigned in the binding with the enzyme for both compounds), including a pattern of small rearrangements in the side chains of the active site residues (Figure 2 and Figure S1 in SI). The dihydrobenzoimidazole moiety is placed into the hydrophilic vertex of the V-shaped enzyme cavity for the substrate, where it engages multiple H bonds with catalytic residues, moreover it binds in front of the FAD cofactor, suggesting π interactions with the isoalloxazine ring.

The presence of the second fluorine on the phenyl ring most likely enhances the hydrophobic interactions of the **2i** amide chain with the aliphatic residues surrounding the tunnel devoted to host the acyl chain of the enzyme substrate.

Table 2
Crystal data collection and refinement statistics.

PDB code	6GOU
Space group	I2
a, *b*, *c* (Å)[a]	147.96 120.64 148.16
α, *β*, γ (°)	90, 95.27 90
Resolution (Å)	2.90
Rsym[b,c] (%)	18.0 (84.2)
CC1/2[c,d]	0.99 (0.83)
Completeness[c] (%)	100 (100)
Redundancy	7.8 (8.1)
Unique reflections	57552
I/σ[c]	11.2 (2.9)
Protein atoms (*N*)	17058
Ligands atoms (*N*)[e]	287
Ramachandran outliers (%)	0.4
Average B value (Å^2)	49.0
Rcryst[f] (%)	21.8
Rfree[f] (%)	25.8
Rms bond length (Å)	0.011
Rms bond angles (°)	1.8

[a]The unit cell of AGPS crystal contains two enzyme dimers.
[b]$R_{sym}=\sum|I_i-<I>|/\sum I_i$, where I_i is the intensity of i^{th} observation and <I> is the mean intensity of the reflection.
[c]Values in parentheses are for reflections in the highest resolution shell.

[d]A cut-off criterion for resolution limits was applied on the basis of the mean intensity correlation coefficient of half-subsets of each dataset ($CC_{1/2}$).
[e]The subunit C does not contain the inhibitor.
[f]Rcryst=∑|Fobs-Fcalc|/∑|Fobs| where Fobs and Fcalc are the observed and calculated structure factor amplitudes, respectively. Rcryst and Rfree were calculated using the working and test sets, respectively.

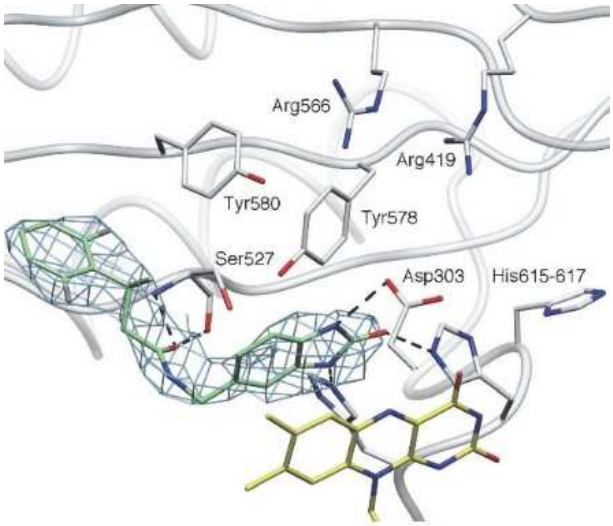

Figure 2. Crystal structure of the AGPS/2i complex. Weighted 2Fo − Fc final electron density map contoured at the 1.2σ level for **2i** bound to subunit B of AGPS. The binding is mediated by specific H bonds (black dashed lines) with the active site residues Asp303, Ser527, His616, and His617.

Molecular modeling studies

Molecular modeling and docking studies have been undertaken to check if different configurations at the chiral centers of Zinc-69435460 (PDB entry code 5AE1, reported in its (*S*,*R*) configuration), **1** (PDB entry code 5ADZ) and **2i** (herein described), both reported as (*S*) enantiomers, could have significant differences in binding energies and thus in predicted inhibition potencies. AGPS complexes were modeled with (*S*,*S*)-Zinc-69435460, (*R*,*S*)-Zinc-69435460, (*R*,*R*)-Zinc-69435460, (*R*)-**1** and (*R*)-**2i** configurations to evaluate their likely formation (see binding mode description and methods in SI). Inspection of the minimized complexes revealed that (*S*,*S*)-Zinc-69435460, (*R*,*S*)-Zinc-69435460, (*R*,*R*)-Zinc-69435460, (*R*)-**1** and (*R*)-**2i** configurations adopt binding modes closely related to the experimental conformations of (*S*,*R*)-Zinc-69435460, (*S*)-**1** and (*S*)-**2i** with no great protein reassembly (Figure 3 and Figure S1, S2 in SI). Analysis of protein-ligand binding free energies re-

ported in Supporting Information Table S5 indicated that (*S*,*S*)-Zinc-69435460, (*R*,*S*)-Zinc-69435460, (*R*,*R*)-Zinc-69435460, (*R*)-**1** and (*R*)-**2i** can bind to AGPS with inhibition potencies comparable to those of their experimental binding configurations.

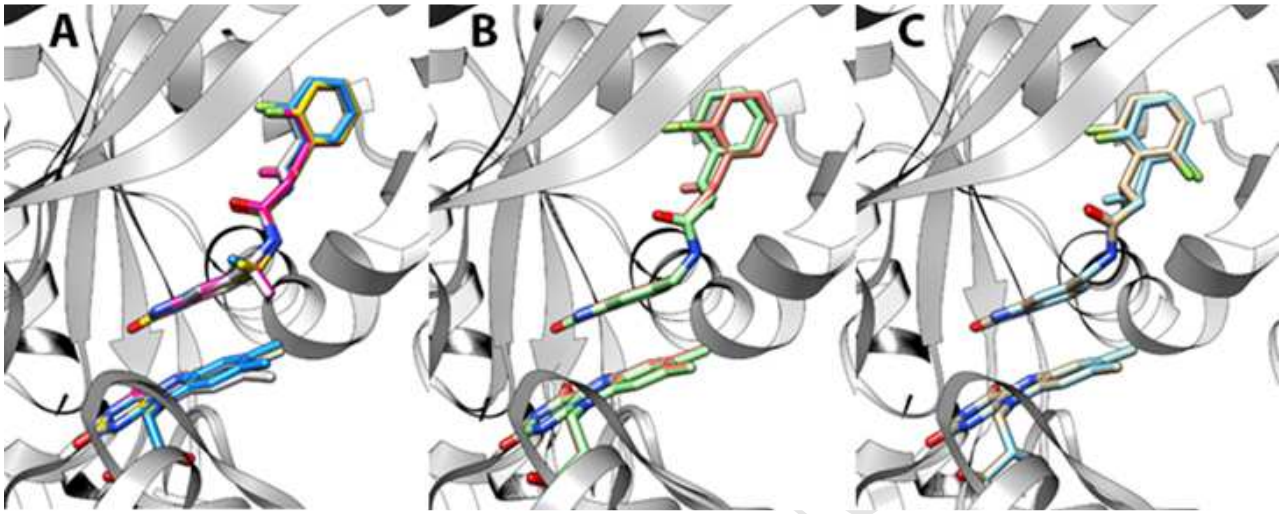

Figure 3. Experimental and modeled AGPS complexes with Zinc-69435460, **1** and **2i**. (A): (*S*,*R*)-Zinc-69435460 (light gray), (*S*,*S*)-Zinc-69435460 (blue), (*R*,*S*)-Zinc-69435460 (yellow) and (*R*,*R*)-Zinc-69435460 (magenta); (B): (*S*)-**1** (light green) and (*R*)-**1** (salmon); (C): (*S*)-**2i** (gold) and (*R*)-**2i** (light blue).

Separation, Chiroptical Characterization and AGPS binding affinity of compound 2i single enantiomers

Although the molecular modelling and docking studies suggested that the two enantiomers of **2i** should not have significant differences in binding energies, we decided, however, to solve **2i** enantiomers by stereoselective HPLC. Semipreparative separations of the enantiomers of **2i** were carried out by HPLC on the 1-cm i.d. Chiralpak IA column under normal phase conditions. The loading effect on the IA column was examined by keeping the concentration of the feed solution constant (i.e. 4.0 mg mL^{-1}) and varying the injection volume from 0.25 to 1.0 mL. As can be noted in the chromatograms depicted in Figure S3, for a sample loading of 4.0 mg the enantiomeric peaks were again well separated and an easy UV signal-guided fractionation of two enantiomers was possible. Both enantiomeric forms were obtained with high ee (> 99%) and in about 90% recovery. Polarimetric

analysis indicated that the less retained enantiomer on the Chiralpak IA column was levorotatory in ethanol solution and the pertinent approximate ORD curve calculated at six wavelengths was monotonic. As shown in Figure S4, the ORD curves of the enantiomers collected on a semipreparative scale were perfectly specular.

The pure collected single enantiomers were screened against AGPS enzyme to assess the influence of chirality in their binding affinity through TermoFAD assay. The TermoFAD assay revealed that, differently from the predicted result, the first eluted enantiomer (-)-**2i** provided +3 °C of Tm increase, while the second one (+)-**2i** gave an higher increase of Tm (+ 6 °C), with the racemate displaying + 5 °C in the same assay. This result will prompt us to investigate on the biological effects of the single eutomer in a next work.

Effects of compounds 2i, 2q and 2s on AGPS enzymatic activity: radioactivity assay

To assess the effect of selected **2** compounds on AGPS catalytic activity, we performed a radioactivity-based enzymatic assay using palmitoyl-DHAP and [1-^{14}C]hexadecanol as substrates and detecting the formation of [1-^{14}C]hexadecyl DHAP as a function of time in the presence of compounds. The catalytically inactive AGPS mutant T578F was used as a control. For the sake of clarity, Figure 4 shows only the effects of **1**, **2i**, **2q** and **2s**.

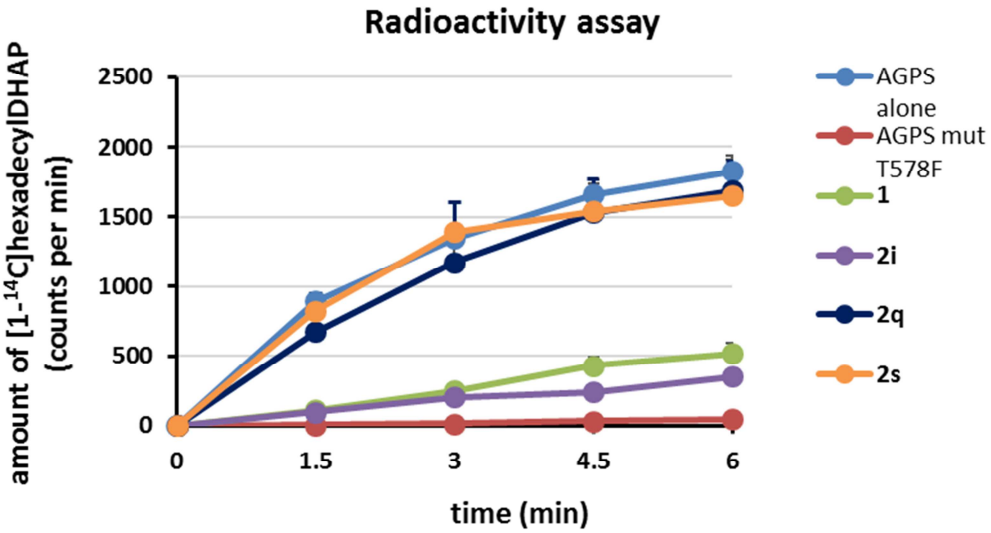

Figure 4. Inhibition of AGPS enzymatic activity was detected by a radioactivity assay using 100 μM palmitoyl-DHAP, 96 μM [1-^{14}C]hexadecanol, and 180 μM inhibitor to detect the formation of [1-^{14}C]hexadecyl-DHAP as a function of time. Controls were performed using AGPS alone and the catalytically inactive AGPS mutant T578F[8] as a positive control. Measurements were performed at least in triplicate.

The effects of **2b-f**,**h**,**j-l**,**t** are reported in Figure S5 in SI. Among the tested compounds, **2k**, **2q**, **2s** and **2t**, which showed very weak or no binding in the ThermoFAD assay, did not display any AGPS inhibition. The 2,6-difluoro-substituted compound **2i**, for which was recorded the highest Tm shift (+ 5 °C), provided the best inhibition profile in the progress curve being as effective as (or slightly more potent than) the reference compound **1** (Figure 4). Enzyme kinetic assays to measure the K_i or IC_{50} values for the identified AGPS inhibitors could not be performed due to the high hydrophobicity of the substrates which, even in presence of surfactants, form micelles and tend to precipitate in the required experimental conditions, impairing accurate determination of the Km and rate values.

Effect of 2i on ether lipid level, on cell migration and survival in aggressive 231MFP breast cancer cells

Compound **2i** was then tested in breast 231MFP cancer cells at 500 μM and resulted able to decrease the levels of ether phospholipids by 50-70% after 24 h of treatment (Figure 5A), as verified by lipidomic analyses through LC-MS/MS. At the same dose, after 6 h **2i** induced 78% decrease of the cell migration rate, higher than that observed with the prototype **1** (500 μM, 48%) after 8 h treatment[13] (Figure 5B). These findings suggest higher potency of **2i** with respect to **1** in a cellular context. Moreover, the ability of **2i** to affect cell survival was also evaluated in the same cell line. After 24 and 48 h of **2i** treatment, the decrease of cell survival provided was 44% and 57%, respectively, in comparison with their corresponding controls (DMSO) (Figure 5C), highlighting that the observed effect on migration is not due to non-specific toxicity.

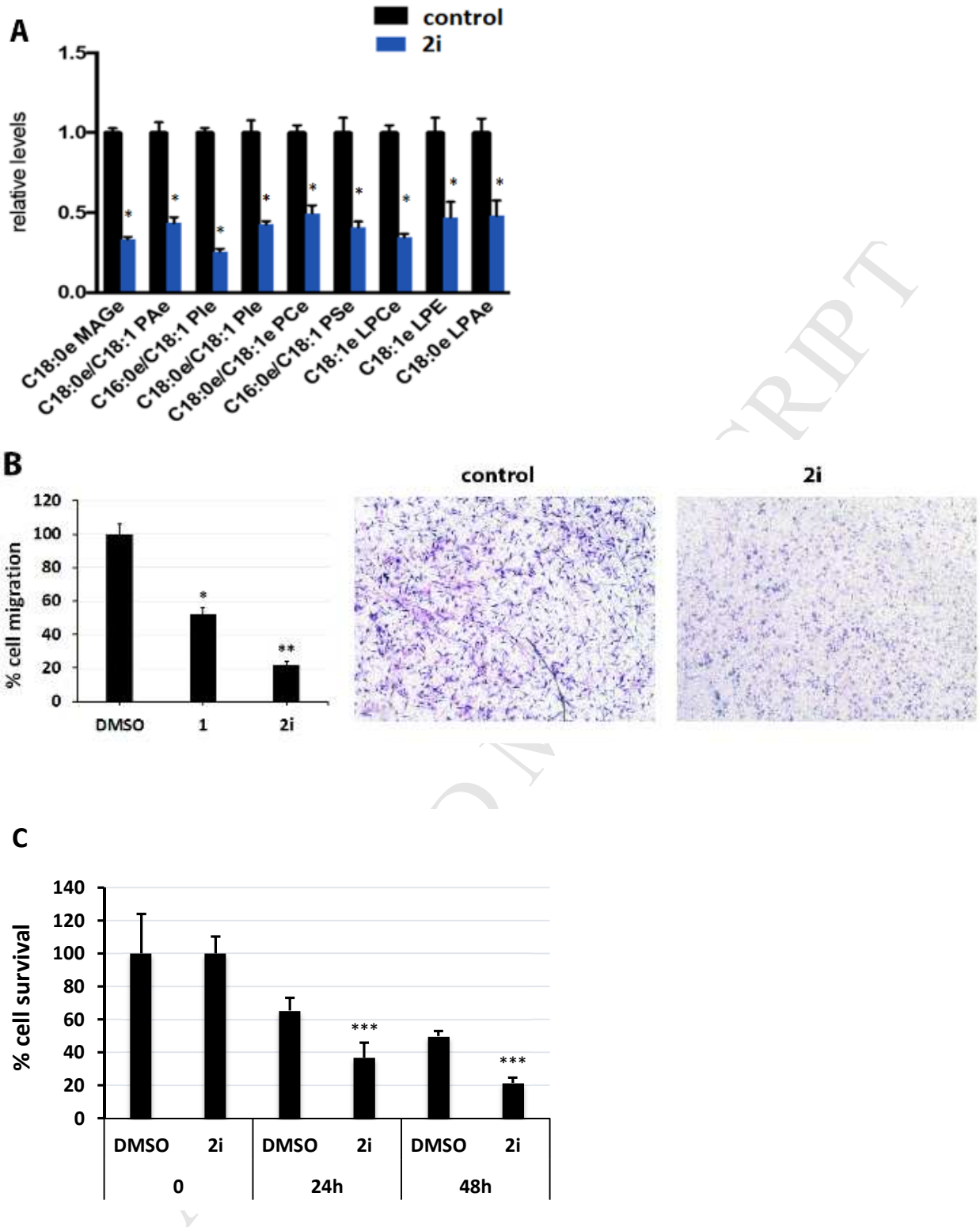

Figure 5. (A) The AGPS inhibitor **2i** lowered ether lipid levels in 231MFP breast cancer cells. The lipidomic profiling data from 231MFP cells treated with vehicle (DMSO) or **2i** (500 μM) for 24 h are shown. Data in bar graphs are the average ± SD. Lipid abbreviations are as follows: MAG, mon-

oalkylglycerol; PA, phosphatidic acid; PI, phosphatidyl inositol; PC, phosphatidylcholine; PS, phosphatidylserine; LPC, lysophosphatidylcholine; LPE, lysophosphatidylethanolamine; LPA, lysophosphatidic acid. Lower case "e" indicates ether phospholipids; (B) effect of **2i** on cell migration rate of breast 231MFP cancer cells after 6 h. Data shown as average ± SD, n = 3−4/group. Significance is represented as *p < 0.05 and as **p < 0.01 related to control groups; (C) Effects of **2i** (500 µM) upon cell survival in 231MFP breast cancer cells after 24 and 48 h treatment. Significance is represented as ***p <0.001 in relation to control groups. Vehicle (DMSO) and **2i** were preincubated with cancer cells before seeding cells into serum-free migration or survival assays (Figure 5B and 5C).

Effects of 2i on proliferation and epithelial-mesenchymal transition (EMT) in PC-3 and MDA-MB-231 cancer cells. Effect of 2i in non-malignant human mesothelial MeT5A cell proliferation

AGPS genetic knockdown in human glioma U87 and hepatic carcinoma HepG2 cells was shown to decrease the expression of oncogenic signaling molecules and to increase the levels of adhesion molecules such as E-cadherin, involved in the control of tumor invasiveness and differentiation.[15] Thus, we investigated whether pharmacological inhibition of AGPS by **2i** could phenocopy its genetic knockdown by modulating EMT. The EMT process is characterized by loss of epithelial and acquisition of mesenchymal features and plays a main role in the acquisition of invasive abilities and chemo resistance in tumors.[16] Prostate PC-3, breast MDA-MB-231 cancer cell lines and MeT5A, a non-tumorigenic cell line used as a control, express detectable levels of AGPS (Figure 6A). A proliferation assay performed with the same cell lines showed negligible effects using **2i** at 100 µM concentration, while a significant reduction of proliferation at 250 µM in PC-3 and mainly in MDA-MB-231 (expressing higher levels of AGPS mRNA, Figure 6A) cells was recorded with **2i** (Figure 6B). In contrast, MeT5A cells were unaffected by the pharmacological treatment even at the highest dose (Figure 6B), thus highlighting cancer specific effects by **2i** treatment.

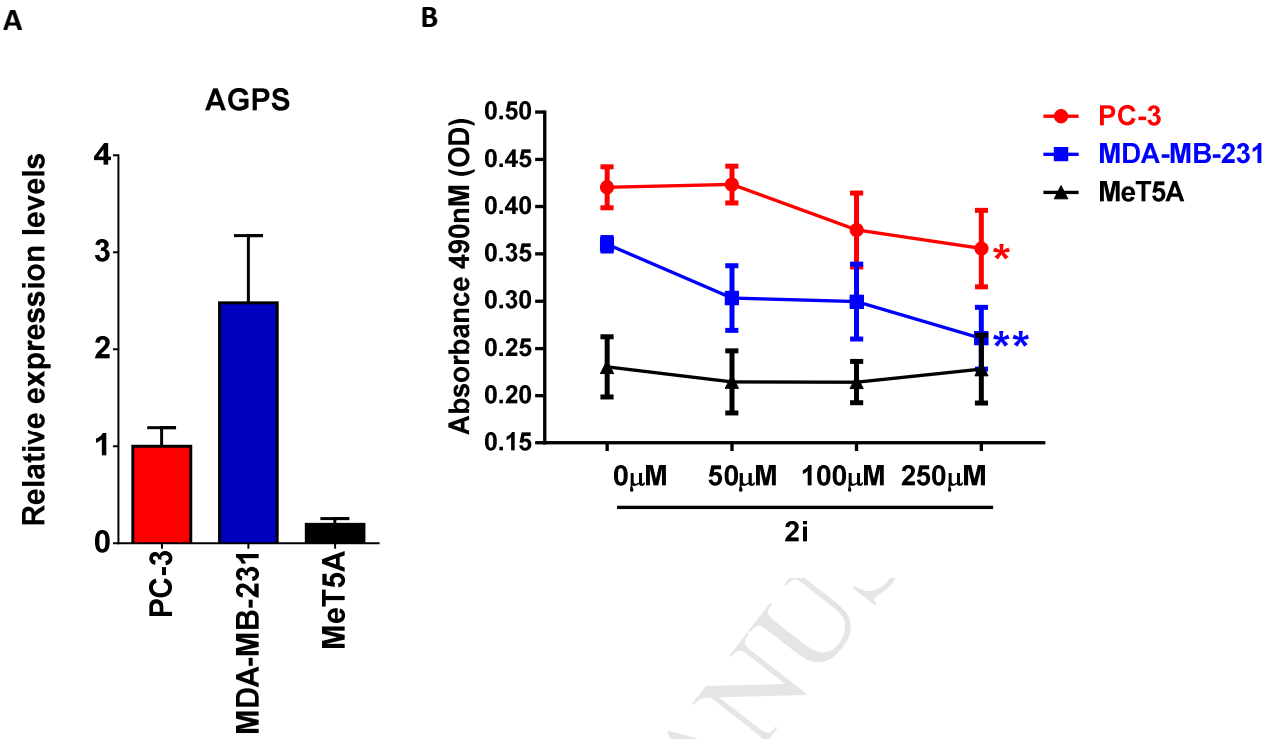

Figure 6. (A) mRNA expression of AGPS in not-treated PC-3, MDA-MB-231 and MeT5A cells to evaluate the basal levels. Quantitative RT–PCR was performed on total RNA. L32 levels were used for normalization. Bars represent ± SEM of seven independent experiments.; (B) Dose−response curves for antiproliferative activity of **2i**, in a dose range (50, 100, 250 μM) on PC-3 and MDA-MB-231 cancer cells and on MeT5A, a non-tumorigenic cell line, after 24 h of treatment. The results represent the average ± SEM of three independent experiments (for a total of 8 measurements). Significance is represented as *$p<0.05$ and **$p < 0.01$ related to control groups.

Thus, we treated PC-3 and MDA-MB-231 cells with **2i** at 50 and 100 μM for 24 h, and we analyzed by RT-PCR the levels of mRNA transcripts of E-cadherin, of its transcriptional regulator Snail, and of matrix metalloproteinase-2 (MMP2), involved in the degradation of basement membrane components and thus implicated in tumor invasion. Compound **1** was used for comparison, whereas **2s** was employed as negative control.

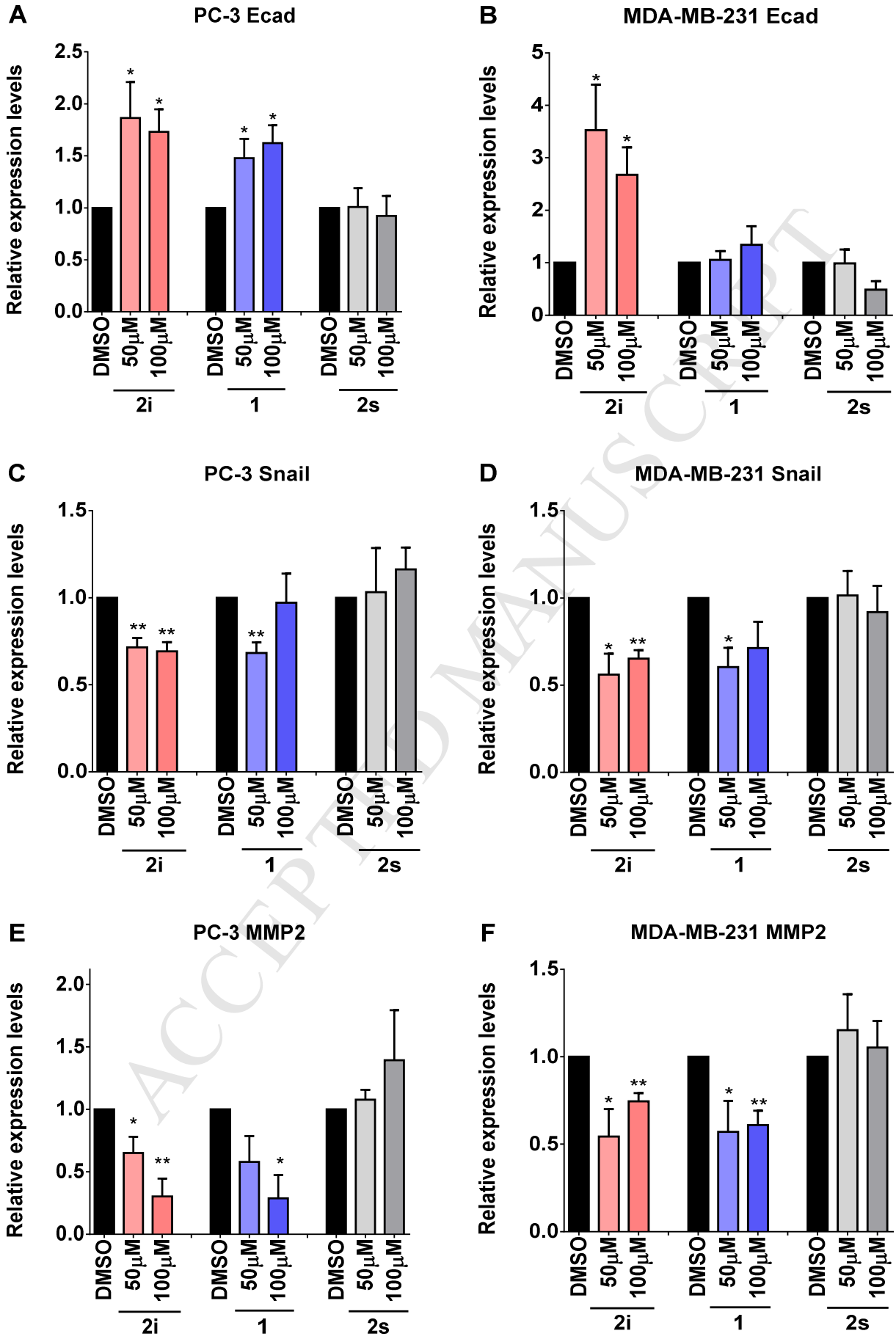

Figure 7. Effects of **2i** (red), **1** (blue), and **2s** (grey, negative control) at 50 and 100 μM on PC-3 and MDA-MB-231 cancer cells after 24 h treatment. Vehicle (DMSO, black) treated cells are used as control. (A-B) E-cadherin transcript quantification via RT-PCR in PC3 and MDA-MB-231 cancer cells; (C-D) Snail transcript quantification via RT-PCR in PC-3 and MDA-MB-231 cancer cells; (E-F) MMP2 transcript quantification via RT-PCR in PC3 and MDA-MB-231 cancer cells. Each data is the mean of at least four independent experiments. Significance is represented as *$p < 0.05$ and as **$p < 0.01$ related to control groups.

The results depicted in Figure 7 show that **2i** is able to increase the level of E-cadherin (Figure 7A-B) as well as to reduce the levels of Snail (Figure 7C-D) and MMP2 (Figure 7E-F) in both the tested cell lines. In the same assays, **2i** displayed similar or higher effects than compound **1** on EMT pathway, whereas **2s** was totally inactive.

AGPS silencing in combination or not with 2i in MDA-MB-231 cells

To exclude any possible off target-dependent EMT modulation by **2i** treatment, we determined the effects on fold expression for AGPS, E-cadherin, Snail, and MMP2, in MDA-MB-231 cells treated with siRNAs against AGPS alone or with a combination of siRNAs against AGPS and **2i** (100 μM). As shown in Figure 8, in all cases very similar results have been obtained, confirming that the observed modulation of **2i** on EMT is specific for AGPS inhibition.

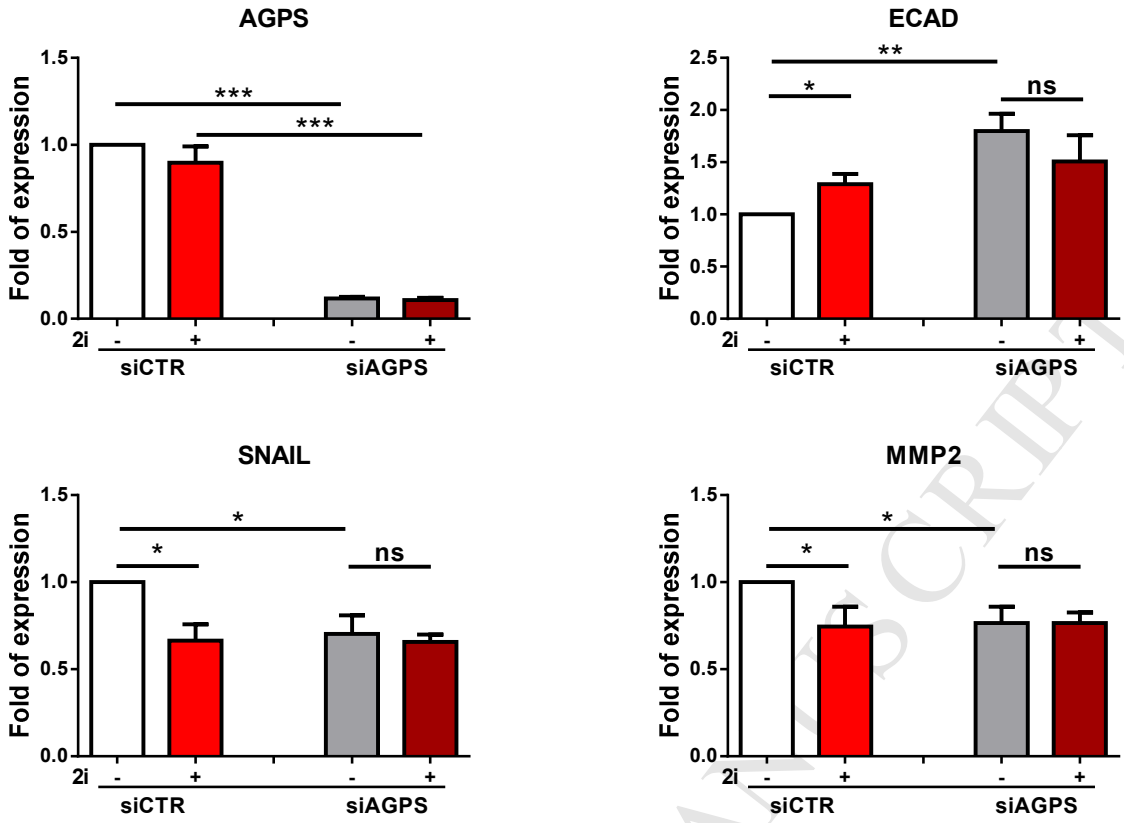

Figure 8. Effects of AGPS silencing either alone or in combination with **2i** treatment (100 µM) in MDA-MB-231 cancer cells. Color code: white, untreated; red, **2i** treatment; grey, siAGPS; brown, **2i** treatment plus siAGPS. Cells interfered for AGPS were treated after 24 h with **2i** or DMSO (control) for 24 additional hours. AGPS, E-cadherin, Snail and MMP2 transcripts quantification has been performed by RT-PCR. Each data is the mean of five independent experiments. Significance is represented as *$p < 0.05$, **$p < 0.01$ and ***$p<0.001$ related to control groups. ns: not significant.

CONCLUSION

Recently the FAD-dependent enzyme AGPS has been shown to be up-regulated across different types of aggressive cancers such as human breast 231MFP, melanoma C8161, and prostate PC-3 cancers.[3] AGPS knockdown led to an overall reduction of ether lipid levels, as well as oncogenic signaling molecules, such as LPAe, PAFe and eicosanoids, and it showed lower tumor growth rates in xenograft mice.[3] The newly established small-molecule screening allowed us to identify and

characterize the first AGPS inhibitor, compound **1**, which recapitulates features of AGPS knockdown. In this study, we described the design and development of some **1** analogs, compounds **2a-l**,**q-u**, designed to investigate structure-activity relationship and to define the pharmacophore elements of the series.

Among structural manipulations applied to the phenylpropionamide and/or the dihydrobenzimidazole moiety of **1** (Figure 1), only the 2,6-difluoro substitution at the phenylpropionamide chain yielded a compound (**2i**) with improved AGPS binding and slightly better inhibitory activity. The crystal structure of the AGPS/**2i** complex revealed that **2i** retains the binding mode observed for **1**, with the second fluorine atom likely enhancing the hydrophobic interactions with the aliphatic residues surrounding the substrate tunnel. In 231MFP breast cancer cells, **2i** reduced the ether phospholipid levels by 50-75% and was more effective than **1** in decreasing cell migration. When tested in PC-3 prostate and MDA-MB-231 breast cancer cells, to check putative modulation of EMT, **2i** increased the levels of E-cadherin and reduced those of Snail, and of MMP2, involved in invasiveness and cancer aggressiveness. Interestingly, these effects were not dependent on reduced proliferation, which was observed only at higher concentration (250 µM) in MDA-MB-231 and to a lesser extend in PC-3 cells. In addition, when tested in non-cancer MeT5A cells compound **2i** displayed negligible effects on cell proliferation, thus revealing cancer specific activity. In the same assays, **1** was often less effective and **2s**, unable to bind and inhibit AGPS, was totally inactive. Genetic knockdown of AGPS by siRNAs in MDA-MB-231 cells produced the same effects as **2i** treatment, and also their combination treatment furnished comparable increase of E-cadherin and reduction of Snail and MMP2 levels, ruling out the possibility of off-target effects by **2i**. Further studies will be conducted to explore the effects of **2i** in a panel of cancer cell lines, with particular emphasis on its effects on migration and invasiveness.

EXPERIMENTAL SECTION

Chemistry. Melting points were determined on a Buchi 530 melting point apparatus and are uncorrected. ^{1}H NMR and ^{13}C NMR spectra were recorded at 400 and 100 MHz, respectively, on a Bruker AC 400 spectrometer; chemical shifts are reported in δ (ppm) units relative to the internal reference tetramethylsilane (Me_4Si). EIMS spectra of all compounds were recorded with a Fisons Trio 1000 spectrometer; only molecular ions (M^+) and base peaks are given. HR-MS spectra of final compounds were recorded with an ESI Orbitrap spectrometer (capillary temperature:275°C, spray voltage 4,0 kV (ESI +) and 3,8 kV (ESI +), sheath gas: 5, tube lens voltage +/- 90 V). The mass spectrometry samples were solubilized in MeOH + 0,01% HCOOH (10^{-5}M). All compounds were routinely checked by TLC and ^{1}H NMR. TLC was performed on aluminum-backed silica gel plates (Merck DC, Alufolien Kieselgel 60 F254) with spots visualized by UV light. All solvents were reagent grade and, when necessary, were purified and dried by standard methods. Concentration of solutions after reactions and extractions involved the use of a rotary evaporator operating at reduced pressure of ca. 20 Torr. Organic solutions were dried over anhydrous sodium sulfate. Elemental analysis has been used to determine the purity of the described compounds, that is >95%. Analytical results are within ±0.40% of the theoretical values. All chemicals were purchased from Sigma-Aldrich, Milan (Italy), or from Alfa Aesar, Karlsruhe (Germany), and were of the highest purity. All the synthetic procedures for the syntheses of **3-12** as well as the chemical and physical data for **2** are reported in SI.

Procedure for the Synthesis of Compounds 3a-d, 3f-l, 4a-d, 4f-l, 5a-l, 6-12

Synthesis of Ethyl 3-(2-Fluorophenyl)-2-methylacrylate (3l).

Triethyl-2-phosphonopropionate (4.83 mmol, 1.2 eq, 1.04 mL) and 2-fluoro benzaldehyde (4.03 mmol, 1.0 eq, 0.42 mL) were added in sequence to a suspension of anhydrous K_2CO_3 (8.06 mmol, 2 eq, 1.11 g) in dry EtOH (10 mL). The reaction mixture was kept stirring at 80 °C for 7 h. After this time the reaction was quenched with water (10 mL), concentrated *in vacuo* and the residue was ex-

tracted with ethyl acetate (3 × 10 mL). The organic layer was dried over Na_2SO_4, filtrated and concentrated *in vacuo*. The crude has been purified by column chromatography on silica gel eluting with *n*-hexane: EtOAc 50:1 to get the compound **3l** as a light yellow oil as a mixture of the two isomers cis:trans=1:2; ^{1}H-NMR ($CDCl_3$, 400 MHz, δ; ppm): δ_H 1.11 (3H, t, *J*= 7.2 Hz, $COOCH_2CH_3$ CIS), 1.38 (6H, *J*= 7.2 Hz, 2 × (3H), t, $COOCH_2CH_3$ TRANS), 2.06 (6H, 2 × (3H), s, C(2)CH_3 TRANS), 2.15 (3H, s, C(2)CH_3 CIS), 4.12 (2H, q, *J*= 6.8 Hz, $COOCH_2CH_3$ CIS), 4.30 (4H, 2 × (2H), q, *J*= 7.2 Hz, $COOCH_2CH_3$ TRANS), 6.75 (1H, s, C(3)*H* CIS), 7.04-7.39 (12 H, m, aromatic protons CIS e TRANS), 7.72 (2H, s, C(3)*H* TRANS) ppm. ^{13}C NMR ($CDCl_3$, 100 MHz, δ; ppm) δ_C: 13.4, 14.7, 60.5, 115.8, 121.9, 124.9, 130.6, 131.0, 132.0, 132.9, 158.6, 169.2 ppm. MS (EI) m/z $[M]^+$: 208.08.

General Procedure for the Synthesis of Ester Intermediates 3a-d, 3f-l.

Trimethyl phosphonacetate (5.21 mmol) was added dropwise to a suspension of NaH (5.21 mmol) in dry THF (8 mL) at 0 °C under inert atmosphere (N_2). After 30 minutes, the appropriate ketone (4.17 mmol) was added to the reaction mixture. The reaction mixture was let to warm slowly to room temperature. The system was kept stirring at room temperature overnight. The next morning the reaction was quenched by addition 1M NH_4Cl (10 mL) and the product was extracted with Et_2O (3 × 10 mL). The combined organic layers were dried over Na_2SO_4, filtered, and concentrated *in vacuo*. The crude was purified by silica gel chromatography eluting with *n*-hexane: EtOAc, 50 :1 to give the pure **3a-d, 3f-l**.

Example: Methyl-3-(2-Chlorophenyl)but-2-enoate (3d).

^{1}H NMR ($CDCl_3$, 400 MHz, δ, ppm): δ_H 2.19 (3H, d, *J*= 1.2 Hz, C(4)H_3 TRANS), 2.52 (3H (2), d, *J*= 1.2 Hz, C(4)H_3 CIS), 3.57 (3H, s, $COOCH_3$ TRANS), 3.78 (3H (2), s, $COOCH_3$ CIS), 5.86 (1H (0.6), d, *J*= 1.6 Hz, C(2)H CIS) 6.04 (1H, d, *J*= 1.6 Hz, C(2)H TRANS), 7.09 (1H, dd *J*= 2.4 Hz, 6.1 Hz, aromatic proton), 7.18-7.20 (1H, m, aromatic proton), 7.24-7.31 (4H, m, aromatic protons CIS+TRANS), 7.39-7.43 (2H, m, aromatic protons CIS+TRANS) ppm. ^{13}C NMR ($CDCl_3$, 100

MHz, δ; ppm) δ_C: 20.7, 51.9, 121.8, 125.3, 129.2, 129.9, 130.7, 133.2, 139.5, 148.6, 166.7 ppm. MS (EI) m/z $[M]^+$ 210.05.

General Procedure for the Synthesis of Arylpropionic Esters Intermediates 4a-d, 4f-l.

A 0.05 M solution of esters **3a-d, 3f-l** (1.31 mmol) in methanol has been reduced under flow conditions (1mL/min) on Pd/C10% catalyst in presence of an H_2 pressure of 10 bar by using H-Cube® (Thales Nano) to give the products in MeOH. The solvent has been evacuated to give the pure products **4a-d, 4f-l**.

Example: Methyl 3-(2,4-Difluorophenyl)butanoate (4h).

^{1}H-NMR ($CDCl_3$, 400 MHz, δ; ppm): δ_H 1.30 (3H, d, *J*= 6.8 Hz, C(3)C*H*$_3$), 2.54-2.60 (2H, dd, *J*= 15.4 Hz, 7.6 Hz, C(2)H), 2.63-2.69 (2H, dd, *J*= 15.4 Hz, 7.6 Hz, C(2)H'), 3.47-3.56 (1H, m, C(2)*H*), 3.63 (1H, s, COOC*H*$_3$), 6.74-6.84 (2H, m, C(6)*H*, C(8)*H*), 7.14-7.20 (1H, m, C(7)*H*) ppm. ^{13}C NMR ($CDCl_3$, 100 MHz, δ; ppm) δ_C: 20.2, 33.0, 38.9, 51.6, 103.6, 111.6, 129.3, 131.1, 153.9, 163.3, 172.1 ppm. MS (EI) m/z $[M]^+$: 214.09.

General Procedure for the Synthesis of Arylpropionic Acids Intermediates 5a-l.

The esters **4a-l** (1.04 mmol) was solubilized in EtOH (2 mL). The system was cooled to 0 °C and a 2M aqueous solution of KOH (4.16 mmol) was added dropwise. The reaction mixture was allowed to warm to room temperature and kept stirring for one hour. After this time the ethanol was removed *in vacuo*. The residual aqueous solution was cooled to 0 °C and titrated with 1M HCl till pH = 1. The product was extracted with ethyl acetate (3 × 10 mL). The combined organic layers were washed with brine (10 mL) and then dried over Na_2SO_4, filtered and concentrated *in vacuo* to give the pure compounds **5a-l**.

Example: 3-(2-Fluorophenyl)pentanoic Acid (5j).

^{1}H NMR (*d*$_6$-DMSO, 400 MHz, δ, ppm): δ_H 0.73 (3H, t, *J*= 7.6 Hz, C(5)H_3), 1.48-1.59 (1H, m, C(4)H), 1.62-1.72 (1H, m, C(4)H'), 2.51-2.55 (1H, dd, *J*= 6.8 Hz, 15.8 Hz, C(2)H), 2.57-2.66 (1H, dd, *J*= 6.8 Hz, 15.8 Hz, C(2)H'), 3.13-3.28 (1H, m, C(3)H), 7.09-7.16 (2H, m, C(8)H, C(10)H),

7.21-7.27 (1H, m, C(9)H), 7.30-7.34 (1H, m, C(11)H), 12.11 (1H, bs, COOH) ppm. MS (EI) m/z $[M]^+$: 196.08.

Synthesis of 1,3-Dimethyl-2-oxo-2,3-dihydro-1*H*-benzo[*d*]imidazo-5-carbonitrile (11).

2-Oxo-2,3-dihydro-1*H*-benzo[*d*]imidazole-5-carbonitrile (1.88 mmol, 1.0 eq, 0.3 g) was solubilized in dry THF (10 mL). The solution was cooled to 0 °C and NaH (4.52 mmol, 2.4 eq, 0.18 g) was added. The reaction mixture was stirred at 0 °C for 20 min. After this time methyl iodide (4.52 mmol, 2.4 eq, 0.64 g) was added dropwise and the system was allowed to warm to room temperature and stirred overnight at room temperature. The next morning the reaction was quenched with water (8 mL). The product was extracted with ethyl acetate (3 × 10 mL). The combined organic layers were washed with a saturated aqueous solution of NaCl (2 × 5 mL), dried over Na_2SO_4 and filtered. The extract was then purified by silica gel chromatography eluting with hexane: ethyl acetate 1: 5 to give the pure compound **11**; Yield: 85%, mp: 204-206 °C (ethanol); ^{1}H-NMR (*d*$_6$-DMSO, 400 MHz, δ; ppm) δ_H: 3.36 (3H, s, -N(1)C*H*$_3$), 3.37 (3H, s, -N(2)C*H*$_3$), 7.33 (1H, d, *J*= 8.4 Hz C(3)*H*), 7.55 (1H, dd, *J*= 1.2 Hz, 8 Hz, C(4)*H*), 7.69 (1H, d, *J*= 1.2 Hz, C(6)*H*) ppm. ^{13}C NMR (*d*$_6$-DMSO, 100 MHz, δ; ppm) δ_C: 26.8, 27.5, 107.7, 111.3, 113.1, 118.3, 128.2, 132.7, 133.5, 155.5 ppm. MS (EI) m/z $[M]^+$: 187.09.

Synthesis of 3-Oxo-1,2,3,4-tetrahydroquinoxaline-6-carbonitrile (12).

Ethyl (4-cyano-2-nitrophenyl)glycinate (1.00 mmol, 1.0 eq, 0.25 g) was dissolved in EtOH (3 mL) and the solution was cooled to 0 °C and was treated with $SnCl_2$ x 2 H_2O (5.01 mmol, 5.0 eq, 1.13 g) and 37 % HCl (0.83 mL). The reaction mixture was stirred at 0 °C for 10 min, then let to warm to room temperature and left under stirring overnight. The next morning the solvent was removed *in vacuo*. The residue was suspended in 20 mL of ethyl acetate and a saturated aqueous solution of Na_2CO_3 was added dropwise till pH=8. The product was extracted with ethyl acetate (3 × 10 mL). The combined organic layers were washed with a saturated aqueous solution of NaCl (2 × 5 mL), dried over Na_2SO_4, filtered and concentrated *in vacuo*. The obtained solid was triturated in petrole-

um ether, filtered and dried to give **12** as pure compound; Yield: 61 %, mp: 190-192°C (acetonitrile); ^{1}H-NMR (*d*$_6$-DMSO, 400 MHz, δ; ppm): δ_H 3.91 (2H, d, *J*= 1.2 Hz, C(2)*H*$_2$), 6.69 (1H, d, *J*= 8 Hz, C(9)*H*), 6.94 (1H, bs, -N*H*CH$_2$CONH-), 6.95 (1H, d, *J*= 1.6 Hz, C(6)*H*), 7.17 (1H, dd, *J*= 1.6 Hz, 8 Hz, C(8)*H*), 10.51 (1H, s, -NHCH$_2$CON*H*-) ppm. ^{13}C NMR (*d*$_6$-DMSO, 100 MHz, δ; ppm) δ_C: 42.6, 105.8, 115.9, 117.9, 118.4, 125.8, 130.5, 138.5, 163.3 ppm. MS (EI) m/z $[M]^+$: 173.05.

Synthesis of 5-Amino-1,3-dihydro-2*H*-benzo[*d*]imidazol-2-one (7).

5-Nitro-1,3-dihydro-2*H*-benzo[*d*]imidazol-2-one (0.837 mmol, 1 eq, 0.15 g) was dissolved in ethanol (5 mL). $SnCl_2 \times 2\ H_2O$ (4.187 mmol, 5 eq, 0.94 g) was added to the solution and the system was cooled to 0 °C. Afterwards, 37 % HCl (0.5 mL) was added dropwise. The reaction mixture was stirred at 0 °C for 10 min, then it was let warm to room temperature and then was heated to 75 °C. The reaction mixture was stirred at this temperature for 3 h and then left overnight (10 h) at room temperature. The next morning the reaction was cooled to 0 °C and quenched by dropwise addition of a saturated aqueous solution of $NaHCO_3$ till pH 7-8. The product was extracted with ethyl acetate (3 × 10 mL). The combined organic layers were washed with a saturated aqueous solution of NaCl (2 × 5 mL) and then dried over Na_2SO_4, filtered and concentrated *in vacuo*. The extract was purified by silica gel chromatography eluting with chloroform: methanol 8:1, to afford the amine **7**; -benzo[d]imidazol-2-one (0.365 mmol, 54.5 mg, Y 44 %). m.p. 253-256 °C (methanol). ^{1}H-NMR (*d*$_6$-DMSO, 400 MHz, δ; ppm) δ_H: 6.21-6.24 (1H, dd, *J*= 2 Hz, 8.2 Hz, C(4)H), 6.29 (1H, d, *J*= 2 Hz, C(2)H), 6.63 (1H, d, *J*= 8 Hz, C(5)H), 10.08 (1H, bs, N(1)H), 10.23 (1H, bs, N(2)H) ppm. ^{13}C NMR (*d*$_6$-DMSO, 100 MHz, δ; ppm) δ_C: 95.4, 106.7, 108.6, 119.9, 130.2, 143.1, 156.4 ppm. MS (EI) m/z $[M]^+$:149.07.

General Procedure for the Synthesis of Amines 6, 8-10.

A 0.05 M solution of carbonitrile derivatives (3.49 mmol) in glacial acetic acid has been let flow (1.5 mL/min) on Pd/C 10% catalyst in presence of an H_2 pressure of 50 bar by using H-Cube® (Thales Nano). The acetic acid was removed under reduced pressure to give the corresponding acetate

salt of the compound. The crude residue was suspended in dry THF and was treated with 10 eq. of HCl (2N in THF). The reaction mixture was stirred for two hours and then the suspension was filtrated giving a solid which was rinsed with petroleum ether to give the pure compound as a colorless solid.

Example: (1*H*-benzo[*d*]imidazol-5-yl)methanamine hydrochloride (8).

^{1}H-NMR (d_6-DMSO, 400 MHz, δ; ppm) δ_H: 4.21 (2H, d, *J*= 5.6 Hz, C(10)H_2), 7.65 (1H, d, *J*= 8.4 Hz, C(4)*H*), 7.86 (1H, d, *J*= 8.4 Hz, C(3)*H*), 8.02 (1H, s, C(6)*H*), 8.56-8.60 (3H, m, CH_2NH_2 and C(8)*H*), 9.42 (1H, s, benzimidazole -N*H*-) ppm. ^{13}C NMR (d_6-DMSO, 100 MHz, δ; ppm) δ_C: 45.9, 114.2, 117.7, 124.8, 136.8, 137.1, 138.0, 143.8 ppm. MS (EI) m/z $[M]^+$: 183.08.

General Procedure for the Amides 2a-l,q-u. The appropriate carboxylic acid **5** (0.4 mmol) was dissolved in dry DMF (3 mL), then 1,1′-carbonyldiimidazole (0.44 mmol) was added and the mixture was stirred at room temperature for 40 min. After this time triethylamine (1.2 mmol) and the proper amine among **6**-**10** (0.6 mmol) was added, and the system was left under stirring at room temperature overnight. The next morning the reaction was judged to be complete by TLC analysis. The reaction was quenched by addition of 10 mL of brine. The product was then extracted with ethyl acetate (3 × 10 mL). The combined organic layers were washed with a saturated aqueous solution of Na_2CO_3 (2 × 5 mL), a 2N HCl aqueous solution (2 × 5 mL) and saturated aqueous solution of NaCl (2 × 5 mL) and then dried over Na_2SO_4, filtered and concentrated *in vacuo*. The obtained white solid was triturated in diethyl ether, filtered and dried to give the pure **2**.

Chemical and Physical Data, ^{1}H NMR, ^{13}C NMR, MS (ESI), and HR-MS (ESI) Data for Compounds 2a-l,q-u.

***N*-((2-Oxo-2,3-dihydro-1*H*-benzo[*d*]imidazol-5-yl)methyl)-3-phenylbutanamide (2a).**

^{1}H NMR (d_6-DMSO, 400 MHz, δ; ppm) δ_H: 1.18 (3H, d, *J*= 6.8 Hz, C(3)CH_3), 3.01-3.04 (2H, m, C(2)H_2), 3.17-3.22 (1H, m, C(3)*H*), 4.18 (2H, d, *J*= 5.6 Hz, C(10)H_2), 6.67 (1H, d, *J*= 8.8 Hz, C(18)*H*), 6.79 (2H, d, *J*= 8 Hz, C(5)*H*, C(9)*H*), 7.16-7.30 (5H, m, C(6)*H*, C(7)*H*, C(8)*H*, C(12)*H*,

C(16)*H*), 8.27 (1H, t, *J*= 5.6 Hz, -N*H*CH_2), 10.54 (1H, s, -N*H*CONH-), 10.56 (1H, s, -NHCON*H*-) ppm. ^{13}C NMR (d_6-DMSO, 100 MHz, δ; ppm) δ_C: 22.1, 36.6, 42.6, 44.4, 108.2, 108.5, 120.7, 126.5, 127.2 (2C), 128.8 (2C), 128.9, 130.2, 132.4, 146.9, 155.9, 171.1 ppm. MS (EI) m/z $[M]^+$: 309.16. HR-MS (ESI) m/z $[M+H]^+$ calculated: 310.1550, found 310.1553.

3-(3-Fluorophenyl)-*N*-((2-oxo-2,3-dihydro-1*H*-benzo[*d*]imidazol-5-yl)methyl)butanamide (2b). ^{1}H NMR (d_6-DMSO, 400 MHz, δ; ppm) δ_H: 1.19 (3H, d, *J*= 7.2 Hz, C(3)CH_3), 2.33-2.45 (2H, m, C(2)H_2), 3.19-3.24 (1H, m, C(3)*H*), 4.17 (2H, d, *J*= 6 Hz, C(10)H_2), 6.65 (1H, d, *J*= 8.8 Hz, C(18)*H*), 6.79 (2H, d, *J*= 8 Hz, C(5)*H*, C(9)*H*), 6.98-7.08 (3H, m, C(8)*H*, C(12)*H*, C(19)*H*), 7.29-7.35 (1H, m, C(7)*H*), 8.24 (1H, t, *J*= 6 Hz, -N*H*CH_2), 10.51 (1H, s, -N*H*CONH-), 10.53 (1H, s, -NHCON*H*-) ppm. ^{13}C NMR (d_6-DMSO, 100 MHz, δ; ppm) δ_C: 22.0, 36.5, 42.6, 44.0, 108.2, 108.4, 113.2, 113.9, 120.0, 123.4, 129.0, 130.2, 130.5, 132.3, 149.8, 155.9, 162.7, 170.8 ppm. MS (EI) m/z $[M]^+$: 327.12. HR-MS (ESI) m/z $[M+Na]^+$ calculated: 350.1275, found: 350.1281.

3-(4-Fluorophenyl)-*N*-((2-oxo-2,3-dihydro-1*H*-benzo[*d*]imidazol-5-yl)methyl)butanamide (2c). ^{1}H NMR (d_6-DMSO, 400 MHz, δ; ppm) δ_H: 1.18 (3H, d, *J*= 6.8 Hz, C(3)CH_3), 2.32-2.41 (2H, m, C(2)H_2), 3.18-3.24 (1H, m, C(3)*H*), 4.17 (2H, m, C(10)H_2), 6.63 (1H, d, *J*= 9 Hz, C(18)*H*), 6.78 (2H d, *J*= 7.6 Hz, C(5)*H*, C(9)*H*), 7.09 (2H, t, *J*= 8.8 Hz, C(12)*H*, C(19)*H*), 7.23-7.27 (2H, m, C(6)*H*, C(8)*H*), 8.23 (1H, t, *J*= 6 Hz, -N*H*CH_2), 10.51 (1H, s, -N*H*CONH-), 10.54 (1H, s, -NHCON*H*-) ppm. ^{13}C NMR (d_6-DMSO, 100 MHz, δ; ppm) δ_C: 22.2, 36.0, 42.6, 44.5, 108.2, 108.4, 115.2, 115.4, 120.0, 128.9 (2C), 129.0, 130.2, 132.3, 142.8, 155.9, 161.1, 170.9 ppm. MS (EI) m/z $[M]^+$: 327.16. HR-MS (ESI) m/z $[M+H]^+$ calculated: 328.1456, found: 328.1467.

3-(2-Chlorophenyl)-*N*-((2-oxo-2,3-dihydro-1*H*-benzo[*d*]imidazol-5-yl)methyl)butanamide (2d). ^{1}H NMR (d_6-DMSO, 400 MHz, δ; ppm) δ_H: 1.16 (3H, d, *J*= 4 Hz, C(3)CH_3), 2.43 (2H, m, C(2)H_2), 3.62 (1H, m, C(3)*H*), 4.20 (2H, bs, C(10)H_2), 6.74 (1H, bs, C(18)*H*), 6.80 (2H, bs, C(9)*H*, C(19)*H*), 7.14 (1H, bs, C(6)*H*), 7.35 (2H, bs, C(7)*H*, C(8)*H*), 7.58 (1H, d, *J*= 8 Hz, C(12)*H*), 8.33 (1H, bs, -N*H*CH_2-), 10.55 (2H, bs, -N*H*CON*H*-) ppm. ^{13}C NMR (d_6-DMSO, 100 MHz, δ; ppm) δ_C: 21.1,

35.5, 42.4, 42.7, 108.2, 108.5, 120.1, 124.1, 127.9, 128.5, 128.5, 129.0, 130.2, 132.3, 133.1, 145.4, 155.9, 170.7 ppm. MS (EI) m/z $[M]^+$: 343.10. HR-MS (ESI) m/z $[M+H]^+$ calculated: 344.1160, found: 344.1175.

3-(2-Bromophenyl)-*N*-((2-oxo-2,3-dihydro-1*H*-benzo[*d*]imidazol-5-yl)methyl)butanamide (2e).

^{1}H NMR (MeOD, 400 MHz, δ; ppm) δ_H: 1.23 (3H, d, *J*= 4 Hz, C(3)CH_3), 2.42-2.48 (1H, dd, J= 8 Hz, 16 Hz, C(2)H_2), 2.56-2.61 (1H, dd, J= 8 Hz, 16 Hz, C(2)H_2), 3.80 (1H, m, C(3)*H*), 4.29 (2H, m, C(10)H_2), 6.84 (1H, d, *J*= 8 Hz, C(18)*H*), 6.93 (2H, d, *J*= 8 Hz, C(9)*H*, C(19)*H*), 7.05 (1H, t, *J*= 8 Hz, C(6)*H*), 7.22-7.32 (2H, m, C(7)*H*, C(12)*H*), 7.52 (1H, d, J= 8 Hz, C(8)*H*) ppm. ^{13}C NMR (d_6-DMSO, 100 MHz, δ; ppm) δ_C: 21.2, 35.5, 42.4, 42.7, 108.2, 108.5, 120.1, 124.1, 127.9, 128.5, 128.5, 129.0, 130.2, 132.3, 133.1, 145.4, 155.9, 170.7 ppm. MS (EI) m/z $[M]^+$: 387.04. HR-MS (ESI) m/z $[M+H]^+$ calculated: 388.0665, 390.0637, found:388.0664, 390.0644.

***N*-((2-oxo-2,3-dihydro-1*H*-benzo[*d*]imidazol-5-yl)methyl)-3-(o-tolyl)butanamide (2f).**

^{1}H NMR (d_6-DMSO, 400 MHz, δ; ppm) δ_H: 1.14 (3H, d, *J*= 6.8 Hz, C(3)CH_3), 2.31 (3H, s, C(5)CH_3), 2.34-2.39 (2H, m, C(2)H_2), 3.40-3.47 (1H, m, C(3)*H*), 4.18 (2H, m, C(10)H_2), 6.66 (1H, d, *J*= 8.4 Hz, C(18)*H*), 6.79 (2H, d, *J*= 7.2 Hz, C(9)*H*, C(19)*H*), 7.05-7.21 (4H, m, C(6)*H*, C(7)*H*, C(8)*H*, C(12)*H*), 8.27 (1H, t, *J*= 5.2 Hz, -N*H*CH_2-), 10.52 (1H, s, -N*H*CONH-), 10.55 (1H, s, -NHCON*H*-) ppm. ^{13}C NMR (d_6-DMSO, 100 MHz, δ; ppm) δ_C: 19.5, 21.6, 31.7, 42.7, 43.6, 108.2, 108.5, 120.0, 125.6, 126.1, 126.6, 128.9, 130.2, 130.5, 132.4, 135.3, 145.0, 155.9, 171.2 ppm. MS (EI) m/z $[M]^+$: 323.15. HR-MS (ESI) m/z $[M+H]^+$ calculated: 324.1707, found: 324.1718.

3-(2-Methoxyphenyl)-*N*-((2-oxo-2,3-dihydro-1*H*-benzo[*d*]imidazol-5-yl)methyl)butanamide (2g).

^{1}H NMR (d_6-DMSO, 400 MHz, δ; ppm) δ_H: 1.11 (3H, d, *J*= 6.4 Hz, C(3)CH_3), 2.34 (1H, dd, *J*= 5.2 Hz, 13.6 Hz, C(2)*H*), 2.40 (1H, dd, *J*= 5.2 Hz, 13.6 Hz, C(2)*H'*), 3.54-3.57 (1H, m, C(3)*H*), 3.78 (3H, s, -OCH_3), 4.15-4.26 (2H, m, C(10)H_2), 6.75 (1H, d, *J*= 8 Hz, C(18)*H*), 6.79-6.82 (2H, m, C(9)*H*, C(19)*H*), 6.89 (1H, t, *J*= 7.6 Hz, C(7)*H*), 6.94 (1H, d, *J*= 7.6 Hz, C(6)*H*), 7.14-7.19 (2H, m,

C(8)*H*, C(12)*H*), 8.27 (1H, bs, -N*H*CH_2-), 10.53 (1H, s, -N*H*CONH-), 10.56 (1H, s, -NHCON*H*-) ppm. ^{13}C NMR (d_6-DMSO, 100 MHz, δ; ppm) δ_C: 20.9, 29.7, 42.6, 43.7, 55.8, 108.2, 108.5, 111.3, 120.1, 120.9, 126.9, 127.4, 129.0, 130.2, 132.5, 134.7, 155.9, 156.9, 171.3 ppm. MS (EI) m/z $[M]^+$: 339.17. HR-MS (ESI) m/z $[M+H]^+$ calculated: 340.1656, found: 340.1664.

3-(2,4-Difluorophenyl)-*N*-((2-oxo-2,3-dihydro-1*H*-benzo[*d*]imidazol-5-yl)methyl)butanamide (2h).

^{1}H NMR (d_6-DMSO, 400 MHz, δ; ppm) δ_H: 1.18 (3H, d, *J*= 6.8 Hz, C(3)H_3), 2.42-2.44 (2H, m, C(2)H_2), 3.41-3.48 (1H, m, C(3)*H*), 4.17 (2H, d, *J*= 5.2 Hz, C(10)H_2), 6.66 (1H, d, *J*= 8 Hz, C(18)*H*), 6.77-6.79 (2H, m, C(9)*H*, C(19)*H*), 7.02 (1H, td, *J*= 2.4 Hz, 8.4 Hz, C(8)*H*), 7.14 (1H, td, *J*= 2.4 Hz, 10.4 Hz, C(12)*H*), 7.34 (1H, q, *J*= 8.8 Hz, C(6)*H*), 8.31 (1H, t, *J*= 5.6 Hz, -N*H*CH_2-), 10.53 (1H, s, -N*H*CONH-), 10.56 (1H, s, -NHCON*H*-) ppm. ^{13}C NMR (d_6-DMSO, 100 MHz, δ; ppm) δ_C: 21.1, 29.8, 42.5, 42.6, 104.0, 108.2, 108.4, 111.7, 120.0, 129.0, 129.4, 129.7, 130.2, 132.3, 155.9, 159.5, 161.9, 170.7 ppm. MS (EI) m/z $[M]^+$: 345.11. HR-MS (ESI) m/z $[M+H]^+$ calculated: 346.1362, found: 346.1380.

3-(2,6-difluorophenyl)-N-((2-oxo-2,3-dihydro-1H-benzo[d]imidazol-5-yl)methyl)butanamide (2i).

^{1}H NMR (d_6-DMSO, 400 MHz, δ; ppm) δ_H: 1.24 (3H, d, *J*= 6.8 Hz, C(3)CH_3), 2.46-2.61 (2H, m, C(2)H_2), 3.63-3.68 (1H, m, C(3)*H*), 4.17 (2H, d, *J*= 5.6 Hz, C(10)H_2), 6.68 (1H, d, *J*= 7.6 Hz, C(18)*H*), 6.78 (2H, t, *J*= 7.6 Hz, C(6)*H*, C(8)*H*), 7.02 (2H, t, *J*= 8.8 Hz, C(12)*H*, C(16)*H*), 7.28 (1H, m, *J*= 7.6 Hz, C(7)*H*), 8.37 (1H, t, *J*= 5.2 Hz, -N*H*CH_2), 10.53 (1H, s, -N*H*CONH-), 10.55 (1H, s, -NHCON*H*-) ppm. ^{13}C NMR (d_6-DMSO, 100 MHz, δ; ppm) δ_C: 19.7, 26.7, 41.4, 42.7, 108.1, 108.5, 112.3 (2C), 120.0, 121.2, 128.7, 128.9, 130.2, 132.3, 155.9, 160.0, 162.5, 170.7 ppm. MS (EI) m/z $[M]^+$: 345.14. HR-MS (ESI) m/z $[M+H]^+$ calculated: 346.1362, found: 346.1376.

3-(2-Fluorophenyl)-*N*-((2-oxo-2,3-dihydro-1*H*-benzo[*d*]imidazol-5-yl)methyl)pentanamide (2j).

^{1}H NMR (d_6-DMSO, 400 MHz, δ; ppm) δ_H: 0.71 (3H, t, *J*= 7.2 Hz, C(21)H_3), 1.47-1.54 (1H, m, C(20)H_2), 1.60-1.67 (1H, m, C (3)*H*), 2.43 (1H, dd, *J*= 8 Hz, 14.2 Hz, C(2)*H*), 2.49 (1H, m, C(2)*H'*), 4.15 (2H, d, *J*= 6 Hz, C(10)H_2), 6.62 (1H, d, *J*= 8 Hz, C(18)*H*), 6.74-6.78 (2H, m, C(9)*H*, C(19)*H*), 7.09-7.16 (2H, m, C(7)*H*, C(8)*H*), 7.21-7.29 (2H, m, C(6)*H*, C(12)*H*), 8.27 (1H, t, *J*= 5.6 Hz, -N*H*CH_2), 10.52 (1H, s, -N*H*CONH), 10.54 (1H, s, -NHCON*H*) ppm. ^{13}C NMR (d_6-DMSO, 100 MHz, δ; ppm) δ_C: 13.1, 22.1, 36.6, 42.7, 45.9, 108.2, 108.6, 112.3 (2C), 119.9, 121.2, 128.6, 128.9, 130.2, 132.3, 156.2, 161.3, 170.5 ppm. MS (EI) m/z $[M]^+$: 341.13. HR-MS (ESI) m/z $[M+H]^+$ calculated: 342.1612, found: 342.1633.

3-(2-Fluorophenyl)-*N*-((2-oxo-2,3-dihydro-1*H*-benzo[*d*]imidazol-5-yl)methyl)-3-phenylpropanamide (2k).

^{1}H NMR (d_6-DMSO, 400 MHz, δ; ppm) δ_H: 2.91 (2H, d, *J*= 7.6 Hz, C(2)H_2), 4.14 (2H, d, *J*= 4.4 Hz, C(10)H_2), 4.78 (1H, t, *J*= 7.6 Hz, C(3)*H*), 6.55 (1H, d, *J*= 7.6 Hz, C(18)*H*), 6.71-6.74 (2H, m, C(9), C(19)), 7.09-7.28 (8H, m, C(6)*H*, C(7)*H*, C(5')*H*, C(6')*H*, C(7')*H*, C(8')*H*, C(9')*H*, C(12)*H*), 7.41 (1H, t, *J*= 7.2 Hz, C(8)*H*), 8.38 (1H, t, *J*= 4.4 Hz, -N*H*CH_2-), 10.53 (1H, s, -N*H*CONH-), 10.56 (1H, s, -NHCON*H*-) ppm. ^{13}C NMR (d_6-DMSO, 100 MHz, δ; ppm) δ_C: (2C under DMSO signal),42.6, 108.1, 108.4, 115.8, 119.9, 124.9, 126.8, 128.0 (2C), 128.6, 128.7 (2C), 128.9, 129.1, 130.1 131.2, 132.1, 143.6, 155.9, 160.4, 170.1 ppm. MS (EI) m/z $[M]^+$: 389.16. HR-MS (ESI) m/z $[M+H]^+$ calculated: 390.1612, found: 390.1632.

3-(2-Fluorophenyl)-2-methyl-*N*-((2-oxo-2,3-dihydro-1*H*-benzo[*d*]imidazol-5-yl)methyl)propanamide (2l).

^{1}H NMR (d_6-DMSO, 400 MHz, δ; ppm) δ_H: 1.03 (3H, d, *J*= 6.4 Hz, C(2)CH_3), 2.61-2.67 (2H, m, C(3)H_2), 2.83 (1H, m, C(2)*H*), 4.13 (1H, dd, *J*= 5.6 Hz, 14.8 Hz, C(10)*H*), 4.21 (1H, dd, *J*= 5.6 Hz, 14.8 Hz, C(10)H_2), 6.65 (1H, d, *J*= 7.6 Hz, C(18)*H*), 6.75-6.80 (2H, m, C(9), C(19)), 7.07-7.15 (2H, m, C(7), C(8)), 7.20-7.27 (2H, m, C(6), C(12)), 8.25 (1H, t, *J*= 5.6 Hz, -N*H*CH_2), 10.52 (1H, s, -N*H*CONH-), 10.54 (1H, s, -NHCON*H*-) ppm. ^{13}C NMR (d_6-DMSO, 100 MHz, δ; ppm) δ_C: 18.2,

32.8, (1C under DMSO signal), 42.6, 108.1, 108.4, 115.5, 120.2, 124.5, 127.1, 128.5, 129.0, 130.2, 131.9, 132.3, 155.9, 161.0, 174.9 ppm. MS (EI) m/z $[M]^+$: 327.13. HR-MS (ESI) m/z $[M+H]^+$ calculated: 328.1456, found: 328.1475.

2-(2,6-Difluorophenyl)-*N*-((2-oxo-2,3-dihydro-1*H*-benzo[*d*]imidazol-5-yl)methyl)propanamide (2q).

^{1}H NMR (d_6-DMSO, 400 MHz, δ; ppm) δ_H: 1.42 (3H, d, *J*= 7.2 Hz, C(2)CH_3), 3.93 (1H, q, *J*= 7.2 Hz, C(2)*H*), 4.22 (2H, d, *J*= 6 Hz, C(9)H_2), 6.78-6.83 (3H, m, C(11)*H*, C(17)*H*, C(18)*H*), 7.06 (2H, t, *J*= 8.4 Hz, (C5)*H*, C(7)*H*), 7.30-7.37 (1H, m, C(6)*H*), 8.22 (1H, t, *J*= 6 Hz, -N*H*CH_2-), 10.53 (1H, s, -N*H*CONH-), 10.56 (1H, s, -NHCON*H*-) ppm. ^{13}C NMR (d_6-DMSO, 100 MHz, δ; ppm) δ_C: 19.7, 41.4, 42.7, 108.1,108.5, 112.4 (2C), 119.7, 121.3, 128.4, 129.7, 130.2, 132.3, 155.7, 161.5 (2C), 171.1 ppm. MS (EI) m/z $[M]^+$: 331.13. HR-MS (ESI) m/z $[M+H]^+$ calculated: 332.1205, found: 332.1223.

3-(2,6-Difluorophenyl)-*N*-(2-oxo-2,3-dihydro-1*H*-benzo[*d*]imidazol-5-yl)butanamide (2r).

^{1}H NMR (d_6-DMSO, 400 MHz, δ; ppm) δ_H: 1.29 (3H, d, *J*= 6.8 Hz, C(3)CH_3), 2.66 (1H, m, C(2)*H*), 2.64-2.79 (1H, m, C(2)*H*), 3.69-3.75 (1H, m, C(3)*H*), 6.79 (1H, d, *J*= 8.4 Hz, C(17)*H*), 6.94 (1H, d, *J*= 8 Hz, C(18)*H*), 7.04 (2H, t, *J*= 8.4 Hz, C(6)*H*, C(8)*H*), 7.27-7.31 (1H, m, C(7)*H*), 7.40 (1H, s, C(11)*H*), 9.82 (1H, s, -N*H*CO-), 10.46 (1H, s, -N*H*CONH-), 10.51 (1H, s, -NHCON*H*-) ppm. ^{13}C NMR (d_6-DMSO, 100 MHz, δ; ppm) δ_C: 19.8, 26.6, 42.3, 101.2, 108.6, 112.2 (2C), 112.4, 121.1, 125.9, 128.9, 130.1, 133.3, 156.0, 160.1, 162.5, 169.4 ppm. MS (EI) m/z $[M]^+$: 331.10. HR-MS (ESI) m/z $[M+H]^+$ calculated: 332.1205, found: 332.1214.

***N*-((1*H*-Benzo[*d*]imidazol-5-yl)methyl)-3-(2,6-difluorophenyl)butanamide (2s).**

^{1}H NMR (MeOD, 400 MHz, δ, ppm) δ_H: 1.36 (3H, d, *J*= 7.2 Hz, C(3)CH_3), 2.68 (2H, d, *J*= 8 Hz, C(2)H_2), 3.78-3.84 (1H, m, C(3)*H*), 4.35 (1H, d, *J*= 14.4 Hz, C(10)*H*), 4.46 (1H, d, *J*= 14.4 Hz, C(10)*H'*), 6.86 (2H, t, *J*= 8.8 Hz, C(6)*H*, C(8)*H*), 7.05 (1H, d, *J*= 8.4 Hz, C(19)*H*), 7.15-7.22 (1H, m, C(7)*H*), 7.45 (1H, s, C(12)*H*), 7.51 (1H, d, *J*= 8.4 Hz, C(18)*H*), 8.15 (1H, s, C(15)*H*) ppm. ^{13}C

NMR (d_6-DMSO, 100 MHz, δ, ppm) δ_C: 19.7, 26.7, 42.7, 48.9, 112.1, 112.4, 113.9, 115.7, 121.2, 121.9 (2C), 128.8, 133.9 (2C), 142.5, 160.1, 162.5, 170.7 ppm. MS (EI) m/z $[M]^+$: 329.12. HR-MS (ESI) m/z $[M+H]^+$ calculated: 330.1412, found: 330.1426.

3-(2,6-Difluorophenyl)-*N*-((1,3-dimethyl-2-oxo-2,3-dihydro-1*H*-benzo[*d*]imidazol-5-yl)methyl)butanamide (2t).

^{1}H NMR (d_6-DMSO, 400 MHz, δ; ppm) δ_H: 1.25 (3H, d, *J*= 7.2 Hz, C(3)CH_3), 2.52-2.58 (2H, m, C(2)H_2), 3.28 (3H, s, C(20)H_3), 3.31 (3H, s, C(21)H_3), 3.62-3.68 (1H, m, C(3)*H*), 4.22-4.27 (2H, m, C(10)H_2), 6.82 (1H, d, *J*= 7.6 Hz, C(18)*H*), 6.94 (1H, s, C(12)*H*), 6.99-7.04 (3H, m, C(6)*H*, C(8)*H*, C(19)*H*), 7.24-7.29 (1H, m, C(7)*H*), 8.40 (1H, t, *J*= 6 Hz, -N*H*CH_2) ppm. ^{13}C NMR (d_6-DMSO, 100 MHz, δ; ppm) δ_C: 19.3, 26.9, 27.4, 30.1, 42.4, 44.0, 108.2, 108.5, 112.4 (2C), 120.1, 121.3, 128.5, 129.1, 130.2, 132.3, 155.4, 161.1 (2C), 173.3 ppm. MS (EI) m/z $[M]^+$: 373.15. HR-MS (ESI) m/z $[M+H]^+$ calculated: 374.1675, found: 374.1694.

3-(2,6-difluorophenyl)-N-((3-oxo-3,4-dihydroquinoxalin-6-yl)methyl)butanamide (2u).

^{1}H NMR (d_6-DMSO, 400 MHz, δ; ppm) δ_H: 1.26 (3H, d, *J*= 7.2 Hz, C(3)CH_3), 2.56 (1H, dd, *J*= 8 Hz, 27 Hz, C(2)*H*), 2.65 (1H, dd, *J*= 8 Hz, 27 Hz, C(2)*H'*), 3.65-3.70 (1H, m, C(3)*H*), 4.30 (2H, d, *J*= 5.6 Hz, C(10)H_2), 6.97-7.04 (3H, m, C(6)*H*, C(8)*H*, C(19)*H*), 7.13 (1H, s, C(12)*H*), 7.25-7.32 (1H, m, C(7)*H*), 7.65 (1H, d, *J*= 8.4 Hz, C(20)*H*), 8.11 (1H, s, N=C*H*CO), 8.57 (1H, t, *J*= 6 Hz, -CON*H*CH_2), 12.4 (1H, bs, N*H*$COCH_2$) ppm. ^{13}C NMR (d_6-DMSO, 100 MHz, δ; ppm) δ: 19.8, 26.6, 41.3, 42.3, 112.2, 112.4, 114.2, 121.1, 122.7, 128.8, 129.1, 131.5, 132.2, 143.3, 151.4, 155.5, 160.0, 162.5, 171.0 ppm. MS (EI) m/z $[M]^+$: 357.11. HR-MS (ESI) m/z $[M+H]^+$ calculated: 358.1367, found: 358.1381

ThermoFAD-based Screening

ThermoFAD experiments were performed with 5 μM AGPS, 180 μM inhibitors in 50 mM HEPES buffer at pH 7.5, 50 mM NaCl, 5% glycerol (20 μL final volume). The temperature gradient was set to 25−70 °C with fluorescence detection every 0.2 °C at 485 ± 30 nm excitation and 625 ± 30 nm

emission for 5 s (BioRad MiniOpticon Real-Time PCR System). To estimate the binding of the identified compounds, the same ThermoFAD protocol was applied by using serial dilutions of the compounds from 500 μM to 10 nM.[13]

Molecular Modelling. See Supplementary material.

Chiral HPLC for enantioseparation of compound 2i

For semipreparative HPLC enantioseparations a Perkin-Elmer (Norwalk, CT,USA) 200 LC pump equipped with a Rheodyne (Cotati, CA, USA) injector, a 2000 μL sample loop, a Perkin-Elmer LC 101 oven and a Waters 484 detector (Waters Corporation, Milford, MA, USA) were used. Specific rotations were measured at 589, 578, 546, 436, 365 and 302 nm by a PerkinElmer polarimeter model 241 equipped with Na/Hg lamps. The volume of the cell was 1 mL and the optical path was 10 cm. The system was set at a temperature of 20°C.

Protein Production and Crystallization

Cavia porcellus AGPS expression and purification were performed according to the methods previously described.[8] Crystals of AGPS in complex with **2i** were obtaining by co-crystallization, pre-incubating AGPS (12 mg mL^{-1}) and **2i** (1 mM) on ice 5 min before setting the plates. Crystals of AGPS/**2i** complex were obtained by sitting-drop vapor diffusion at 20 °C mixing the pre-incubated AGPS/**2i** solution and 2−6% wt/vol PEG 1500 in 100 mM 4-(2-hydroxyethyl)-1-piperazineethanesulfonic acid (Hepes) at pH 7.0-7.5 and washed in cryo-protectant solution (30 wt %/vol PEG 1500 in 100 mM Hepes, pH 7.0-7.5) with inhibitor before freezing. Crystal structure determination was carried out with programs of the CCP4 suite.[17]

Targeted Lipidomic Analyses

Metabolite measurements were conducted using previous procedures with minor modifications.[3] Cancer cells were grown in serum-free media for 24 h to minimize the contribution of serum-derived metabolites to the cellular profiles. Cells were treated with 2i (500 μM) for 24 h. Cancer cells (1×10^6 cells/6 cm dish or 2×10^6 cells/6 cm dish) were washed twice with phosphate bu□er sa-

line (PBS), harvested by scraping, and isolated by centrifugation at 1400g at 4 °C, and cell pellets were flash frozen and stored at −80 °C until metabolome extractions. Lipid metabolites were extracted in 4 mL of a 2:1:1 mixture of chloroform: methanol/phosphate (buffered saline, pH 7.4, 50 mM) with the inclusion of internal standards C12:0 dodecylglycerol (10 nmol) and pentadecanoic acid (10 nmol). Organic and aqueous layers were separated by centrifugation at 1000g for 5 min, and the organic layer was collected. The aqueous layer was acidified (for metabolites such as LPA) by adding 0.1% formic acid, followed by the addition of 2 mL of chloroform. The mixture was vortexed, and the organic layers were combined, dried down under N_2, and dissolved in 120 μL of chloroform, of which 10 μL was analyzed by both single reaction monitoring (SRM)-based LC-MS/MS or untargeted LC-MS. LC separation was achieved with a Luna reverse-phase C5 column (50 mm × 4.6 mm with 5 μm diameter particles, Phenomenex). MS analysis was performed with an electrospray ionization (ESI) source on an Agilent 6430 QQQ LC-MS/MS. Representative metabolites were quantified by SRM of the transition from precursor to product ions at associated collision energies.

Cell Culture and Cell Migration Studies

231MFP cells were grown as previously described.[3] PC-3 and MDA-MB-231 were cultured in DMEM media containing 10% (vol/vol) FBS and maintained at 37 °C with 5% (wt/vol) CO_2. MeT5A cells were cultured in M199 media containing 10% (vol/vol) FBS and maintained in the same conditions. Migration assays were performed in Transwell chambers (Corning) coated with collagen as previously described.[24] 231MFP cell migration was measured after 24 h of 500 μM **2i** treatment.

Cell proliferation assay

Cell viability was measured using a CellTiter 96® AQueous One Solution Cell Proliferation Assay (MTS) (Promega) following manufacturer's instructions. Briefly, $20x10^3$ PC-3, MDA-MB-231 or MeT5A cells were seeded in 96 well tissue culture plates. After 24 h, culture medium containing **2i**

at reported concentrations was added. After 24 h, 20 µL of AQueous One Solution Reagent was added to each well and absorbance was recorded at 490 nm. Three independent experiments (for a total of 8 measurements) were performed.

RNA Extraction, Reverse Transcription and Real-time Polymerase Chain Reaction RNAs were extracted by RNeasy Mini Kit (Qiagen GmbH, Hilden, Germany) and reverse transcribed with iScriptTM c-DNA Synthesis Kit (Bio-Rad Laboratories Inc., Hercules, CA, USA). cDNAs were amplified by a qPCR reaction using GoTaq qPCR Master Mix (Promega, Madison, WI, USA) and the oligonucleotides pairs specific for the target genes analysed. Relative amounts, obtained with $2^{(-\Delta Ct)}$ method, were normalized with respect to the housekeeping gene human L32. The primers used are described in SI.

siRNA interference

Cells were transfected with equal amounts of siRNAs against AGPS (AGPS#1 AAUUCGCUCAAACAUUCCUUG; AGPS#2 AAGGAUUUCUUCUCUAGCAGC) or a scramble control (GGCUACGUCCAGGAGCGCACC) by RNAiMAX reagent (Invitrogen), according to commercial protocol. A total of 100 pmol siRNAs were used for each condition.

24 hours post transfection, cells were treated with **2i** (final concentration 100 µM or with an equal volume of DMSO) without detaching them from the plates.

Cells were collected 24 h post-treatment with **2i** for RNA analysis.

ASSOCIATED CONTENT

Supporting Information. Experimental for chemistry (synthesis and chemical and physical data for compounds **6-10**), molecular modelling studies, biochemistry (radioactive assay for compounds **2b-f**,**h**,**j-l**,**t**), biology (siRNA primers sequences). Additional crystallographic data. Authors will release the atomic coordinates and experimental data upon article publication.

AUTHOR INFORMATION

Corresponding Author

*A.Mattevi: phone, +39 0382 985525; fax, +39 0382 528496; E-mail, andrea.mattevi@unipv.it.
*A.Mai: phone, +39 06 49913392; fax, +39 06 49693268; E-mail, antonello.mai@uniroma1.it
*S.Valente.: phone, +39 06 49913237; fax, +39 06 49693268; E-mail, sergio.valente@uniroma1.it
Author Contributions
[1]G. Stazi, C. Battistelli and V. Piano share first authorship of this article.
Present Address
[d]Department of Mechanistic Biology, Max Planck Institute for Molecular Physiology, Otto-Hahn-Strasse 11, 44227 Dortmund, Germany.

ACKNOWLEDGMENT

We are grateful to Claudia Binda for her assistance in AGPS TermoFAD assays. This work was supported by PRIN 2015 (prot. 20152TE5PK) (A.Mai, A.Mattevi), AIRC Fellowship 18022 (V.P.), AIRC 2016 (n. 19162) (A.Mai) and AIRC 2016 (n. 18843) (M.T.) funds.

ABBREVIATIONS

acyl-DHAP, acyl-dihydroxyacetone phosphate; AGPS, alkylglyceronephosphate synthase; DHAP, dihydroxyacetone phosphate; DMEM: Dulbecco′s modified Eagle′s medium; DMF: *N*,*N*-dimethylformamide; DMSO: dimethylsulfoxide; EIMS, electron ionization mass spectrometry; EMT: epithelial to mesenchymal transition; ESI, electrospray ionization; FAD: flavin adenine dinucleotide; FBS: fetal bovine serum; HPLC; high performance liquid chromatography; HRMS: high resolution mass spectrometry; LC-MS: liquid chromatography-mass spectrometry; LPA, lysophosphatidic acid; LPAe, lysophosphatidic acid ether; LPC, lysophosphatidylcholine; LPE, lysophosphatidylethanolamine; MAG, monoalkylglycerol; MMP2: metalloproteinase 2; ORD: optical rotatory dispersion; PA, phosphatidic acid; PAFe, platelet activating factor ether; PBS: phosphate buffer saline; PC, phosphatidylcholine; PEG: polyethylene glycol; PI, phosphatidyl inositol; PS, phosphatidylserine; q-PCR: quantitative polymerase chain reaction; RT-PCR: teal time-polymerase chain reaction; siRNA: small interference RNA; SRM: single reaction monitoring; THF: tetrahydrofuran; TLC: thin layer chromatoghraphy.

REFERENCES

1. Snyder, F.; Wood, R. Alkyl and alk-1-enyl ethers of glycerol in lipids from normal and neoplastic human tissues. *Cancer Res* **1969,** 29, 251-7.

2. Roos, D. S.; Choppin, P. W. Tumorigenicity of cell lines with altered lipid composition. *Proc Natl Acad Sci U S A* **1984,** 81, 7622-6.

3. Benjamin, D. I.; Cozzo, A.; Ji, X.; Roberts, L. S.; Louie, S. M.; Mulvihill, M. M.; Luo, K.; Nomura, D. K. Ether lipid generating enzyme AGPS alters the balance of structural and signaling lipids to fuel cancer pathogenicity. *Proc Natl Acad Sci U S A* **2013,** 110, 14912-7.

4. Zhu Y, Liu XJ, Yang P, Zhao M, Lv LX, Zhang GD, Wang Q, Zhang L. Alkylglyceronephosphate synthase (AGPS) alters lipid signaling pathways and supports chemotherapy resistance of glioma and hepatic carcinoma cell lines. Asian Pac J Cancer Prev. 2014;15(7):3219-26.

5. Murray M, Hraiki A, Bebawy M, Pazderka C, Rawling T. Anti-tumor activities of lipids and lipid analogues and their development as potential anticancer drugs. Pharmacol Ther. 2015 Jun;150:109-28.

6. Razeto, A.; Mattiroli, F.; Carpanelli, E.; Aliverti, A.; Pandini, V.; Coda, A.; Mattevi, A. The crucial step in ether phospholipid biosynthesis: structural basis of a noncanonical reaction associated with a peroxisomal disorder. *Structure* **2007,** 15, 683-92.

7. de Vet, E. C.; Hilkes, Y. H.; Fraaije, M. W.; van den Bosch, H. Alkyl-dihydroxyacetonephosphate synthase. Presence and role of flavin adenine dinucleotide. *J Biol Chem* **2000,** 275, 6276-83.

8. Nenci, S.; Piano, V.; Rosati, S.; Aliverti, A.; Pandini, V.; Fraaije, M. W.; Heck, A. J.; Edmondson, D. E.; Mattevi, A. Precursor of ether phospholipids is synthesized by a flavoenzyme through covalent catalysis. *Proc Natl Acad Sci U S A* **2012,** 109, 18791-6.

9. Wang, D.; Dubois, R. N. Epoxyeicosatrienoic acids: a double-edged sword in cardiovascular diseases and cancer. *J Clin Invest* **2012,** 122, 19-22.

10. Mills, G. B.; Moolenaar, W. H. The emerging role of lysophosphatidic acid in cancer. *Nat Rev Cancer* **2003,** 3, 582-91.

11. Kendall, A. C.; Nicolaou, A. Bioactive lipid mediators in skin inflammation and immunity. *Prog Lipid Res* **2013,** 52, 141-64.

12. Forneris, F.; Orru, R.; Bonivento, D.; Chiarelli, L. R.; Mattevi, A. ThermoFAD, a Thermofluor-adapted flavin ad hoc detection system for protein folding and ligand binding. *FEBS J* **2009,** 276, 2833-40.

13. Piano, V.; Benjamin, D. I.; Valente, S.; Nenci, S.; Marrocco, B.; Mai, A.; Aliverti, A.; Nomura, D. K.; Mattevi, A. Discovery of Inhibitors for the Ether Lipid-Generating Enzyme AGPS as Anti-Cancer Agents. *ACS Chem Biol* **2015,** 10, 2589-97.

14. Rotili, D.; Tarantino, D.; Nawrozkij, M. B.; Babushkin, A. S.; Botta, G.; Marrocco, B.; Cirilli, R.; Menta, S.; Badia, R.; Crespan, E.; Ballante, F.; Ragno, R.; Este, J. A.; Maga, G.; Mai, A. Exploring the role of 2-chloro-6-fluoro substitution in 2-alkylthio-6-benzyl-5-alkylpyrimidin-4(3H)-ones: effects in HIV-1-infected cells and in HIV-1 reverse transcriptase enzymes. *J Med Chem* **2014,** 57, 5212-25.

15. Zhu, Y.; Zhu, L.; Lu, L.; Zhang, L.; Zhang, G.; Wang, Q.; Yang, P. Role and mechanism of the alkylglycerone phosphate synthase in suppressing the invasion potential of human glioma and hepatic carcinoma cells in vitro. *Oncol Rep* **2014,** 32, 431-6.

16. Nieto, M. A. Epithelial plasticity: a common theme in embryonic and cancer cells. *Science* **2013,** 342, 1234850.

17. Winn, M. D.; Ballard, C. C.; Cowtan, K. D.; Dodson, E. J.; Emsley, P.; Evans, P. R.; Keegan, R. M.; Krissinel, E. B.; Leslie, A. G.; McCoy, A.; McNicholas, S. J.; Murshudov, G. N.; Pannu, N. S.; Potterton, E. A.; Powell, H. R.; Read, R. J.; Vagin, A.; Wilson, K. S. Overview of the CCP4 suite and current developments. Acta Crystallogr D Biol Crystallogr 2011, 67, 235-42.

Highlights

1. AGPS enables the acyl/alkyl exchange of acyl-dihydroxyacetone phosphate
2. AGPS is up-regulated across different types of aggressive and metastatic tumors
3. AGPS inactivation reduce ether lipids and oncogenic signaling molecules levels
4. AGPS inhibitor 2i decreases ether lipids, cell migration and survival
5. Inhibitor 2i specifically impaired EMT through E-cadherine, Snail, Mmp2 modulation